J. Fluid Mech. (2006), *vol.* 552, *pp.* 311–343.
doi:10.1017/S0022112006008822 Printed in the United Kingdom

Capillary drainage of an annular film: the dynamics of collars and lobes

By J.R. LISTER[1], J.M. RALLISON[1], A.A. KING[2], L.J. CUMMINGS[2] AND O.E. JENSEN[2]

[1]Institute of Theoretical Geophysics, Department of Applied Mathematics and Theoretical Physics, University of Cambridge, Wilberforce Road, Cambridge CB3 OWA, UK

[2]School of Mathematical Sciences, University of Nottingham, Nottingham NG7 2RD, UK

(Received 31 August 2004 and in revised form 22 September 2005)

This paper considers the capillary drainage of a thin annular film on the inside or outside of a circular cylinder of radius a. A film of uniform thickness and axial length greater than πa suffers a Rayleigh instability and evolves to form an axisymmetric structure in which the film thickness varies with axial distance. The fluid is gathered into *collars*, having axial length $2\pi a$, and shorter *lobes*; the pressure within each collar or lobe is spatially uniform and adjacent collars and lobes are separated by thin necks. We examine numerically the evolution of this structure and demonstrate that, for sufficiently short cylinders, lobes drain into collars as described by Hammond (*J. Fluid Mech.* vol. 137, 1983, p. 363). For longer cylinder lengths we find that, in spite of the energetic advantage, neighbouring collars do not drain into one another, and that the neck region between adjacent collars is governed by a similarity solution of the thin-film equation having axial length that varies as $t^{-1/2}$ after time t, and film thickness that varies as t^{-1}, which is different from that found by Jones & Wilson (*J. Fluid Mech.* vol. 87, 1978, p. 263).

We also find a new phenomenon: a collar can spontaneously and episodically translate back and forth along the cylinder, on each occasion consuming the lobe ahead and leaving a smaller daughter lobe behind. This motion takes place on several different timescales: the relatively rapid translation is governed by Landau–Levich equations; the collision with a neighbouring collar is governed by the similarity equation for the neck regions ahead and behind; and the delay between one episode of translation and the next is governed via the Landau–Levich equation by a slow peeling process. Asymptotic results for each of the processes of translation, collision and peeling are obtained and are compared with a full numerical solution. Each episode of translation reduces the thickness of the daughter lobe by a factor 0.115, and successive translations back and forth give rise to a lobe thickness that decays on average and on very long timescales like $t^{-1/2}$.

A thin film of fluid trapped beneath a two-dimensional drop sedimenting towards a rigid horizontal plane is described by the same evolution equation, and analogous lobe and collar dynamics are found (Lister, Morrison & Rallison, *J. Fluid Mech.* vol. 552, 2006, p. 345).

1. Introduction

A liquid film coating the interior or exterior of a sufficiently long cylinder will redistribute under the action of surface tension so that its thickness varies axially. Ultimately, such a film may form an occlusive liquid plug in a tube or a large bead

on the outside of a fibre. There are numerous applications for which a fundamental understanding of such flows is important, including two-phase flows in porous media (Olbricht 1996), liquid-lining flows in lung airways (Grotberg & Jensen 2004), coating flows (Quéré 1999) and technologies such as microfluidics and heat exchangers (Allen & Hallinan 2001). Thin-film flow on a cylinder can generally be described in relatively simple terms through a single nonlinear evolution equation derived using lubrication theory (Oron, Davis & Bankoff 1997) and there is considerable mathematical interest in the PDEs governing this and related problems (e.g. Bertozzi & Pugh 1998; Bertozzi, Grun & Witelski 2001). They fall into the class of long-wave-unstable gradient-flow systems that typically exhibit coarsening behaviour of the sort found in Cahn–Hilliard systems. Here we investigate the long-time evolution of a thin axisymmetric liquid layer on a cylinder, and show how viscous effects can generate surprisingly complex dynamics over very long timescales, preventing the system from coarsening to its expected minimum energy state.

The early- and intermediate-time dynamics of a thin viscous film coating a cylinder have been widely investigated. A uniform thin film may be deposited on the interior of a cylinder behind a slowly moving bubble or drop (Bretherton 1961), or on the exterior of a cylinder by withdrawal from a liquid bath (Quéré 1999). Surface tension then drives the film towards new configurations with lower surface area via the Rayleigh instability, at a rate determined by viscous forces. The early-time behaviour can be described with a linear stability analysis, which reveals the wavelength of the fastest growing disturbances (Goren 1962). The subsequent nonlinear evolution is captured using lubrication theory (Hammond 1983), which yields a leading-order evolution equation (see (2.5) below) that (because the relationship between interfacial curvature and film thickness is linearized) applies to films both on the inside and the outside of a cylinder. Typically the film redistributes into annular *collars* (of length $2\pi a$, where a is the tube radius) separated by *lobes* (of length less than $2\pi a$). Each collar and lobe is a local capillary equilibrium shape. Slow drainage of liquid from a stationary lobe into a neighbouring stationary collar is controlled by a thin quasi-steady transition region of the kind identified by Jones & Wilson (1978) and which arises widely in thin-film problems (e.g. Wu & Weinbaum 1982; Braun & Fitt 2003; Jensen, Chini & King 2004). In relatively short domains, for which there is no significant collar migration, such drainage persists until the film thins so much that intermolecular (e.g. van der Waals) forces become important.

Numerous additional effects can influence the dynamics of films coating cylinders. For thick films, nonlinearities in the relationship between curvature and film thickness are significant. Films on the interior of a cylinder can form an occlusive liquid plug (Everett & Haynes 1972), the formation of which can be captured either with a thin-film equation extended to include exact curvature terms (Gauglitz & Radke 1988) or with full numerical simulations (e.g. Johnson *et al.* 1991; Newhouse & Pozrikidis 1992; Hagedorn, Martys & Douglas 2004). Thick films on the exterior of cylinders can bead up into large drops (Quéré 1999). Weak gravity acting parallel to the cylinder axis then causes collars, plugs or drops to drift downwards, and intricate merging dynamics may ensue (Quéré 1990; Trifonov 1992; Kalliadasis & Chang 1994; Kerchman & Frenkel 1994; Chang & Demekhin 1999; Jensen 2000; Kliakhandler, Davis & Bankoff 2001). Shear, for example arising in core–annular flow, also leads to complex collar dynamics (e.g. Aul & Olbricht 1990; Kerchman 1995; Joseph *et al.* 1997), although sufficiently strong forcing (either gravity or shear) can suppress the primary Rayleigh instability in the weakly nonlinear regime (e.g. Frenkel *et al.* 1987; Halpern & Grotberg 2003). Gravity acting normal to the cylinder, either with

rotation of the cylinder around its axis at a rate large enough for inertial effects to be significant (e.g. Moffatt 1977; Thoroddsen & Mahadevan 1997; Hosoi & Mahadevan 1999), or in the absence of rotation (de Bruyn 1997; Jensen 1997; Weidner, Schwartz & Eres 1997), again leads to axially non-uniform structures that can drift along the cylinder.

The destabilizing force acting on a thin film coating a cylinder is provided by pressure gradients associated with azimuthal curvature gradients. Gravity or intermolecular forces can act on a planar thin film in a similar fashion. The Rayleigh–Taylor instability of a liquid layer adjacent to a horizontal surface, for example a heavy layer coating a ceiling (e.g. Yiantsios & Higgins 1989; Newhouse & Pozrikidis 1990) or a buoyant film trapped beneath a sedimenting drop (e.g. Jones & Wilson 1978; Yiantsios & Davis 1990; Ascoli, Dandy & Leal 1990; Pozrikidis 1990), is described (in one spatial dimension) by an evolution equation equivalent to that studied by Hammond (1983), with pendent drops (for example) being analogous to collars. In particular, the simulations of Yiantsios & Higgins (1989) provide evidence that a thin film dripping off a ceiling does not approach its minimum energy state and that its final state is dependent on the initial conditions; the numerical results in this study did not describe accurately the evolution of the system over very long times, however. The rupture of a thin film on a planar surface is conveniently modelled by allowing both for destabilizing long-range van der Waals forces (attracting the interface to the solid surface) and stabilizing short-range repulsive forces, so that the breakup of a film into isolated drops can be modelled without having to deal with contact-line singularities explicitly (e.g. Sharma & Khanna 1998). In this framework, an individual drop with small but non-zero contact angle comes into equilibrium with a neighbouring ultra-thin film of a nearly constant thickness set by a balance between the long-range and short-range intermolecular forces. Multiple isolated drops on a long domain drift and merge over long timescales and ultimately the system coarsens to its minimum energy state (e.g. Mitlin 1993; Glasner & Witelski 2003). Both the Rayleigh–Taylor and the film-rupture problems offer experimentally accessible opportunities to investigate long-time pattern formation and coarsening dynamics in two dimensions (e.g. Limat *et al.* 1992; Fermigier *et al.* 1992; Limary & Green 2003).

In this paper we revisit Hammond's (1983) evolution equation describing the axisymmetric coating of a cylinder, allowing the film to adjust under the action of surface tension and viscosity alone. The evolution of this system turns out to be more intricate than the system described by Glasner & Witelski (2003), because the lobes between collars are non-uniform and can become arbitrarily thin. High-resolution finite-difference simulations (adaptive in both space and time) show that, contrary to expectation, the canonical quasi-steady Jones–Wilson draining flow found between *stationary* collars and lobes is not a universal feature in extended domains over very long times. Instead, new unsteady draining regimes emerge, associated with episodes of axial translation of collars along the cylinder in which the lobe ahead is consumed and a smaller daughter lobe left behind. Each episode ends with a collision with a neighbouring collar and a new episode is initiated on a much longer timescale by the completion of a slow peeling process from the daughter lobe. A foretaste of some of this dynamics is provided in figure 1.

The problem is formally defined and described in § 2, and illustrative numerical results are presented in § 3. These results motivate asymptotic analyses of the special case of adjacent stationary collars in § 4 and of the generic processes of translation, collision and peeling in §§ 5–7. Among the surprises are that colliding collars do not coalesce, despite the energetic advantage of doing so, and that this dissipative system

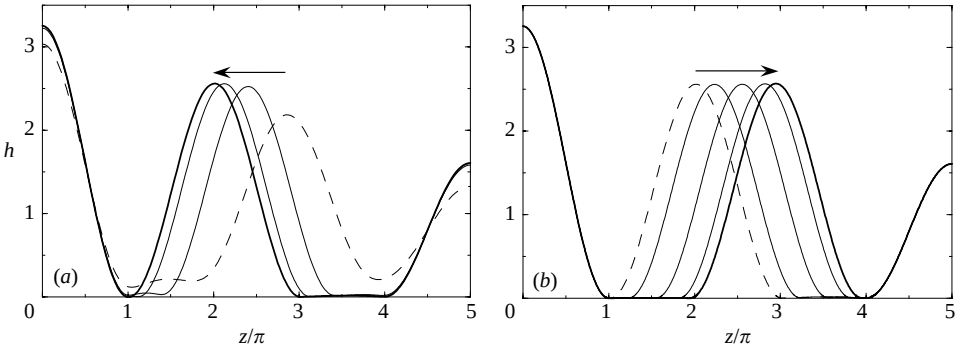

FIGURE 1. The evolution of a thin film of thickness h on a cylinder of length 5π. The details of the calculation and the non-dimensionalization are given in §§2 and 3. (*a*) Time $t = 10^2$ (dashed), 10^3, 10^4 and 10^6 (bold); (*b*) $t = 2.1 \times 10^6$ (dashed), 2.18, 2.2, 2.22 and 2.3×10^6 (bold). Between $t = 10^2$ and 10^5 the central collar slides to the left from $2 < z/\pi < 4$ into $1 < z/\pi < 3$, consuming the lobe ahead of it and leaving a smaller daughter lobe behind in $3 < z/\pi < 4$. Between $t = 2.1 \times 10^6$ and 2.3×10^6, the collar slides back to the right leaving an even smaller daughter lobe in $1 < z/\pi < 2$. The episodic sliding motion is halted by collisions with the collars pinned at the ends of the domain by the boundary conditions and is reinitiated by a peeling process that cannot be seen on this scale.

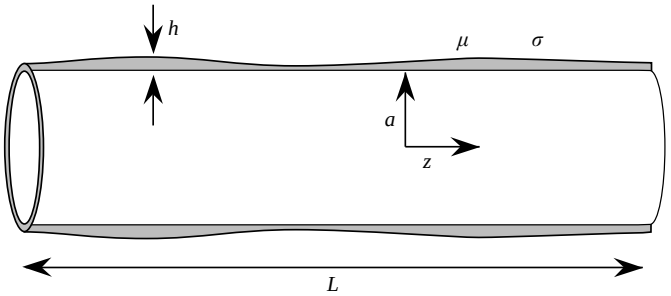

FIGURE 2. Definition sketch. A rigid cylinder of radius a is coated by a thin axisymmetric layer of liquid of viscosity μ, surface tension σ and thickness $h(z, t)$, where z is the axial coordinate. The length of the domain is L.

can exhibit oscillatory dynamics over very long timescales. The implications for the asymptotic behaviour of this system, and for related problems, are explored in §§8 and 9.

The following companion paper (Lister, Morrison & Rallison 2006) describes a closely related problem in which many similar features arise, namely the evolution of the film trapped beneath a drop sedimenting towards a rigid horizontal plane.

2. Problem description

2.1. *Governing equation*

Consider a rigid cylinder of radius a coated by a thin axisymmetric layer of liquid of viscosity μ and thickness $h(z, t)$, where z is the axial coordinate (figure 2). We assume that $h \ll a$ and $h_z \ll 1$. It follows that the interfacial curvature

$$\kappa = \frac{1}{R\left(1 + R_z^2\right)^{1/2}} - \frac{R_{zz}}{\left(1 + R_z^2\right)^{3/2}}, \tag{2.1}$$

where $R(z,t) = a + h(z,t)$, can be approximated by

$$\kappa = \frac{1}{a} - \frac{h}{a^2} - h_{zz}. \tag{2.2}$$

We assume that gravity is negligible and that both the external pressure and the surface tension σ are uniform. The flow in the film is then driven solely by the capillary pressure gradient

$$p_z = \sigma\kappa_z = -\sigma(a^{-2}h + h_{zz})_z. \tag{2.3}$$

We assume that inertia is negligible and, using $h \ll a$ and $h_z \ll 1$ again, make the usual lubrication approximations to obtain

$$h_t + \frac{\sigma}{3\mu}(h^3(a^{-2}h + h_{zz})_z)_z = 0. \tag{2.4}$$

Equation (2.4) also describes the evolution of a thin layer of fluid coating the inside of a hollow cylinder of internal radius a (Hammond 1983). In this case $R = a - h$, the interfacial curvature is approximated by $\kappa = a^{-1} + a^{-2}h + h_{zz}$ and the capillary pressure is $-\sigma\kappa_z$. The dynamical effects of a second fluid in the centre of the cylinder are negligible provided its viscosity is much less than $\mu a/h$. Differences between the evolution of internal and external coating layers only appear if the small $O(h_z^2)$ correction terms are retained in the curvature.

By scaling h with a typical initial thickness $\hat{h}$, z with a, p with $\sigma\hat{h}/a^2$ and t with $\mu a^4/(\sigma\hat{h}^3)$, we obtain the dimensionless evolution equation

$$h_t + \tfrac{1}{3}(h^3(h_z + h_{zzz}))_z = 0. \tag{2.5}$$

This paper describes the long-time evolution of solutions of (2.5). Numerical calculations were performed on a finite domain $0 \leqslant z \leqslant L$ subject to the symmetry boundary conditions

$$h_z = h_{zzz} = 0 \qquad \text{at} \qquad z = 0, L. \tag{2.6}$$

2.2. *Collars, lobes and energy*

It is straightforward to show from (2.5) that a uniform film of thickness h_0 is linearly unstable on an infinite domain to wavenumbers $k < 1$ with a maximum growth rate $h_0^3/12$ at $k = 2^{-1/2}$. This reflects the Rayleigh instability, which drives the film toward a state of minimum surface energy and hence minimum surface area. By expanding the relevant axisymmetric integrals to $O(\hat{h}^2/a^2)$, it can be shown that, on a finite domain with boundary conditions such as (2.6) or periodicity, the problem of minimizing surface area subject to the constraint of constant volume is equivalent in the thin-film approximation to

$$\text{minimize } E \equiv \frac{1}{2}\int_0^L \left(h_z^2 - h^2\right) \mathrm{d}z \quad \text{subject to } \int_0^L h \,\mathrm{d}z = \text{const.} \tag{2.7}$$

An equivalent form is obtained by Yiantsios & Higgins (1989). Under the same boundary conditions, (2.5) can be used to show that the rate of dissipation $\Phi = -\mathrm{d}E/\mathrm{d}t$ is given by

$$\Phi = \frac{1}{3}\int_0^L h^3(h_z + h_{zzz})^2 \,\mathrm{d}z \geqslant 0. \tag{2.8}$$

There exist equilibrium configurations of the film corresponding to solutions in which the pressure

$$p = -(h + h_{zz}) \tag{2.9}$$

is a constant, P, and hence

$$h = A\cos(z - z_0) - P, \tag{2.10}$$

where $A \geqslant 0$, and A and z_0 are constants. The case $P > -A$ corresponds to a finite drop of fluid having the form of an annular ring of length $\ell = 2\cos^{-1}(P/A) < 2\pi$, which meets the cylinder at a non-zero contact angle. We call this structure a *lobe*. The case $P = -A$ gives a finite drop of length $\ell = 2\pi$, which meets the cylinder tangentially; we call this a *collar*. (The case $P < -A$ describes a neutrally stable perturbation to a uniform film, but will not be relevant to the subsequent discussion.) Strictly speaking, these collar and lobe solutions have zero film thickness at their edges and such contact points could not move under (2.5) (see, for example, King & Bowen 2001 and references therein). For our initial conditions (with $h > 0$ at $t = 0$) the film thickness remains everywhere non-zero for all times and we shall use the terms collar and lobe more loosely to refer to local solutions given at leading order by (2.10) which match onto regions of much smaller, but non-zero, thickness at their edges. Since, for long times, we find that almost all of the fluid is gathered into collars that do not merge, conservation of mass guarantees that under our non-dimensionalization A remains of order unity for each collar.

Integration gives the volume V and energy E of a collar or lobe as

$$V = P\left[2\tan\left(\tfrac{1}{2}\ell\right) - \ell\right], \qquad E = P^2\left[\tan\left(\tfrac{1}{2}\ell\right) - \tfrac{1}{2}\ell\right] = \tfrac{1}{2}PV. \tag{2.11a, b}$$

Thus, for a collar, $P = -V/2\pi$ and $E = -V^2/4\pi$.

Equation (2.11a, b) shows that the energy of a given volume of fluid is decreased by transferring fluid from higher-pressure lobes or collars to lower-pressure lobes or collars, and by increasing the lengths of lobes until they become collars. Such considerations hint at the possible evolution of (2.5), but prove to be only part of the story.

The simulations of Hammond (1983) show that the linear instability of a uniform film develops nonlinearly into a sequence of lobes and collars, with the lobes emptying slowly into the adjacent lower-pressure collars through a very thin connecting neck (see for example figure 3a, c below). Hammond analyses the long-time drainage of a lobe by noting that in a neck $h \ll 1$ and thus, at leading order, the neck evolves quasi-statically. Because the neck region is short, $h_z \ll h_{zzz}$ and (2.5) shows that the leading-order flux

$$q = \tfrac{1}{3}h^3 h_{zzz} \tag{2.12}$$

through the neck is spatially constant. The neck, with position $z_n = z_0 - \pi$, say, must match to the lobe with a prescribed small contact angle $\theta(t) > 0$ on one side, and to the collar (2.10) on the other, and so (2.12) is solved with boundary conditions $h \to (z_n - z)\theta$ as $z - z_n \to -\infty$ and $h \to \frac{1}{2}A(z - z_n)^2 + O(1)$ as $z - z_n \to \infty$ (where the limits $z - z_n \to \pm\infty$ are interpreted in the asymptotic sense as meaning the overlap between inner and outer solutions). As noted by Jones & Wilson (1978), this problem has a unique solution for which $q \propto \theta^5$ and the minimum neck thickness scales as θ^2. Since, however, the volume of the lobe is proportional to θ and is lost to the collar at a rate proportional to θ^5, it follows that $\theta \propto t^{-1/4}$ giving a minimum neck thickness $t^{-1/2}$.

Hence on Hammond's analysis if the collars cannot move then the ultimate configuration as $t \to \infty$ will be one of isolated collars with lobes of zero volume (i.e. $h \to 0$) between them. If the collars can move then the most energetically favourable configuration is for the collars to merge to form a single large collar. Somewhat

surprisingly, we show below that, although collar motion removes fluid from the lobes faster than the Hammond drainage mechanism, the collars do not merge.

3. The dynamics of collars and lobes

3.1. *Numerical scheme*

The numerical scheme was designed to address two features of the solutions.

First, in order to maintain resolution of the very small lengthscales of the necks between the collars and lobes, the scheme uses an adaptive spatial grid in which the grid point spacing is inversely proportional to $1 + h^{-1/2}$. The factor $h^{-1/2}$ is chosen to reflect the fact that a neck of thickness $h \ll 1$ has lengthscale $O(h^{1/2})$. As time-integration proceeds, the grid points are occasionally redistributed using quintic polynomial interpolation, with new ones added, according to the current variation of film thickness. Typical calculations begin with 400 points when $h = O(1)$ and require 4000 points for resolution of late times.

Second, the natural timescale for evolution of (2.5) on a lengthscale Δz is $O(\Delta z^4/h^3)$. With $\Delta z \propto h^{1/2}$ this gives a timescale $O(h^{-1})$ and shows that the evolution of the thin necks occurs on a very much longer timescale than adjustment of the collars to their equilibrium shape. In order to examine the long-time evolution of this stiff system, (2.5) was discretized semi-implicitly using the current values of h^3 and the future values of the pressure $p = -(h + h_{zz})$. This gives relaxation of the collars to the correct equilibria even if large time steps are taken to follow the slow evolution of the necks. Typical calculations used a time step chosen so that h did not change by more than 0.2 % at any point. Further details of the discretization are given in the Appendix.

The numerical scheme was verified against independent calculations made using the NAG routine D02NCF, which is a fully implicit stiff integrator. The scheme described here was much faster and more stable at late times, owing to the semi-implicit treatment.

3.2. *Numerical results*

In order to illustrate the relevance of lobes and collars to the long-time dynamics, we first present calculations made with initial condition

$$h(z, 0) = 1 + 0.1\cos(\pi z/L). \tag{3.1}$$

The subsequent evolution is found to depend strongly on the value of L.

If $L \leqslant \pi$ then the domain is too short to include unstable wavenumbers and a film of uniform thickness is stable.

If $L > \pi$ then the initial perturbation to a uniform film grows, and is found to develop nonlinearly into a number of collars and lobes. The positions of the centres of these collars and lobes will, in general, depend on the choice of initial condition, though on short domains there is little or no room for flexibility and the arrangement of collars and lobes is fixed. As explained below, the arrangement is always fixed for $L < 3\pi$.

3.2.1. *Short domains*

For the initial conditions (3.1) we find that the arrangement happens to be fixed for $L < 3.72\pi$, and the consequent evolution is relatively straightforward. Profiles of h at different times are shown in figure 3 for various values of L in this range and also for the special case $L = 4\pi$ for which the arrangement becomes fixed after a long initial

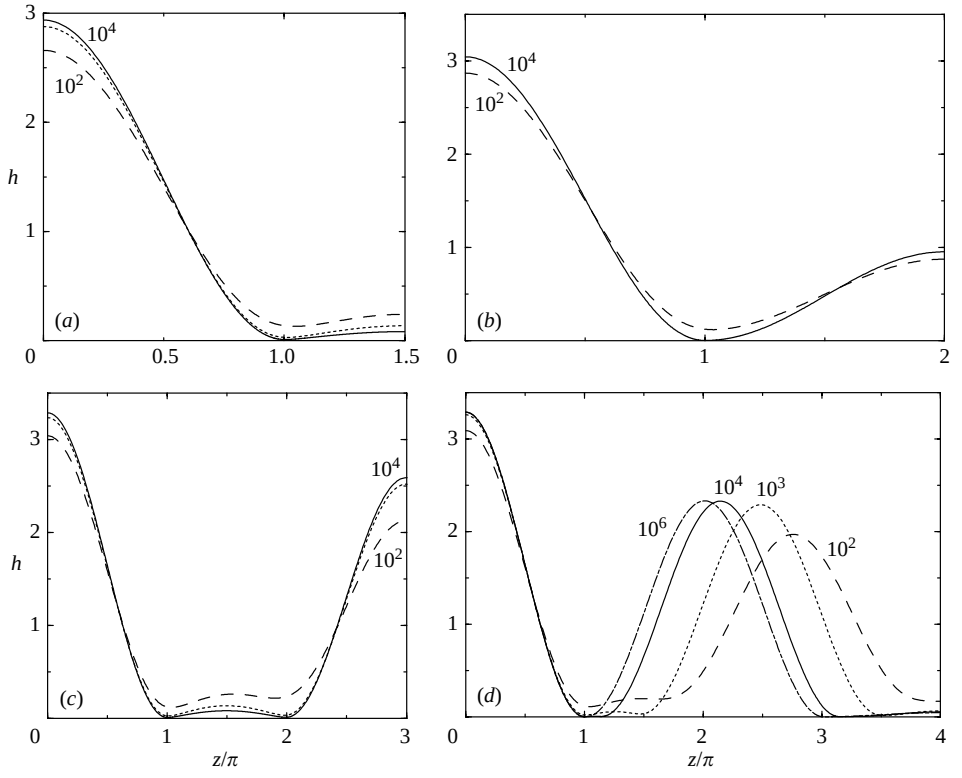

FIGURE 3. Solutions of (2.5) with initial condition (3.1) for various short domain lengths L. The symmetry boundary conditions (2.6) imply the other half of the collar (length $\ell = 2\pi$) or lobe ($\ell < 2\pi$) at each end of the domain. (*a*) $L = 1.5\pi$ at $t = 10^2, 10^3, 10^4$. The lobe (implied) in $1 < z/\pi < 2$ drains into the collar in $-1 < z/\pi < 1$. (*b*) $L = 2\pi$ at $t = 10^2, 10^4$. Adjacent collars do not drain into each other. (*c*) $L = 3\pi$ at $t = 10^2, 10^3, 10^4$. The lobe in $1 < z/\pi < 2$ drains into the collars on either side. (*d*) $L = 4\pi$ at $t = 10^2, 10^3, 10^4, 10^6$. The collar in $2 < z/\pi < 4$ at $t = 10^2$ slides left, engulfing a lobe, until it occupies $1 < z/\pi < 3$. It leaves a collar in $3 < z/\pi < 5$. This arrangement of adjacent collars then persists indefinitely.

transient. For $L = 1.5\pi$ there is half a collar in $0 \leqslant z \leqslant \pi$ having amplitude of order unity, together with half a lobe of much smaller amplitude in $\pi \leqslant z \leqslant L$ (the other halves are implied by the boundary conditions). The collar and lobe are stationary. The same qualitative behaviour, with a single half-collar and a single half-lobe, is obtained whenever $\pi < L < 2\pi$. For $L = 2\pi$ there is room for exactly two half-collars; for $2\pi < L < 3.72\pi$ there are half-collars in $0 \leqslant z \leqslant \pi$ and $L - \pi \leqslant z \leqslant L$ with a lobe between them; and for $L = 4\pi$ there is room for exactly two half-collars with a collar between them. Once half-collars have formed at the ends of the domain, the boundary conditions (2.6) keep them pinned and the geometric constraints of the short domain determine the rest of the structure. For the case $L = 4\pi$ it takes until $t \approx 10^5$ for the arrangement of two half-collars and a collar to be attained, but the arrangement then persists indefinitely.

Figure 4 shows the time-dependence of the minimum thicknesses between the various collars and lobes. For $L = 1.5\pi$ and $L = 3\pi$ the minima all lie between a lobe and a collar, and the asymptotic variation is $h \propto t^{-1/2}$ in accordance with the similarity solution of Jones & Wilson (1978) and Hammond (1983) described earlier: a spatially uniform flux proportional to $t^{-5/4}$ drains from the lobe through the neck into the

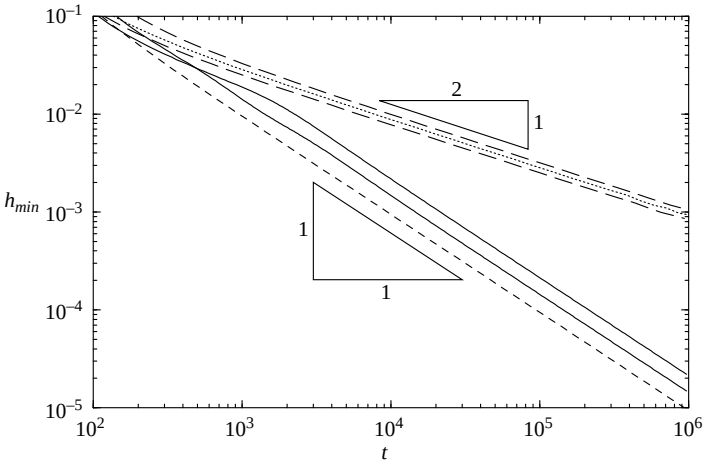

FIGURE 4. The time-dependence (log-log scale) of the various minima in figure 3 for $L = 1.5\pi$ (dotted), 2π (dashed), 3π (long-dashed) and $L = 4\pi$ (solid). In every instance, where a collar is adjacent to a lobe $h \propto t^{-1/2}$, but where two collars are adjacent $h \propto t^{-1}$.

adjacent collar, so that the volume of the lobe decreases like $t^{-1/4}$. In contrast, for $L = 2\pi$ and $L = 4\pi$ the minima all lie between two collars, and the asymptotic variation is $h \propto t^{-1}$. There is found to be no net flux through the minimum and, instead, a flux proportional to $t^{-5/2}$ is expelled from the neck into the adjacent collars so that the minimum thickness of the neck decreases rapidly. Similarity solutions for this new behaviour will be presented in § 4.

3.2.2. *Longer domains*

It may seem that the new similarity solutions are only relevant to domain lengths that permit an integer number of stationary collars or half-collars to fill the domain completely. In fact, whenever $L > 4\pi$ there is sufficient room for one or more collars, which are in the interior of the domain and not pinned by the boundary conditions, to move sideways, eventually colliding with other collars or half-collars. This sideways motion is generally accompanied by the 'eating up' of a lobe by a collar (see figure 1 and § 5). However, since the collar has fixed length 2π it must leave behind another lobe as it moves. This daughter lobe is found to have smaller volume than that consumed, and thus the collar gains volume as it moves; the growth of the collar provides the energy source for the motion. Sliding and colliding collars form the generic behaviour for $L > 4\pi$, and the collisions are also described by new similarity solutions (see § 6). The overall dynamics are, however, considerably more complex than those on a short domain.

For the initial conditions (3.1) these more complex dynamics also occur for $3.72\pi \leqslant L < 4\pi$, with the computational domain containing a pinned half-collar, a moving collar, and one or two lobes. The boundary, $L = 3.72\pi$, between this behaviour, and the simpler dynamics of two half-collars and a lobe, which is observed for $2\pi \leqslant L < 3.72\pi$, depends on the initial conditions and was found numerically by bisection. (Consideration of the length requirements of these two arrangements of half-collars, collars and lobes suggests that the boundary will, in general, lie in the range $3\pi < L < 4\pi$.)

As a representative example of the case $L > 4\pi$, figures 1 and 5–7 show results for $L = 5\pi$. By $t = 100$ the initial film thickness (3.1) has already developed into

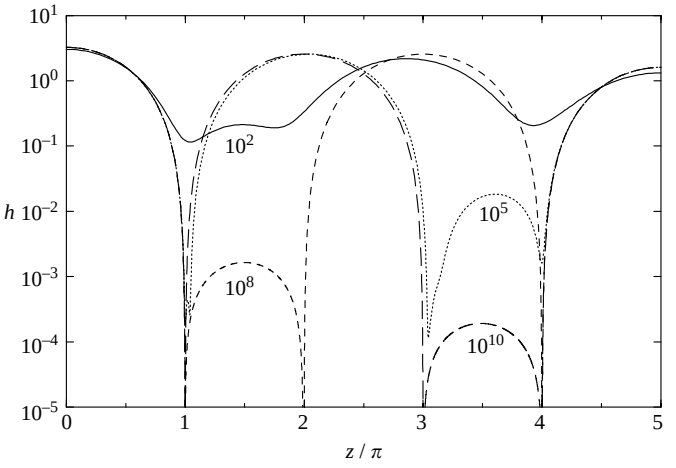

FIGURE 5. The film thickness (logarithmic scale) for $L = 5\pi$ at $t = 10^2$ (solid), 10^5 (dotted), 10^8 (dashed) and 10^{10} (long-dashed). The central collar flips between $1 < z/\pi < 3$ and $2 < z/\pi < 4$, while the daughter lobe left in $1 < z/\pi < 2$ or $3 < z/\pi < 4$ decreases in thickness and volume by a factor of about 10 on each flip. The motion of the central collar during the first two flips is shown in more detail in figure 1.

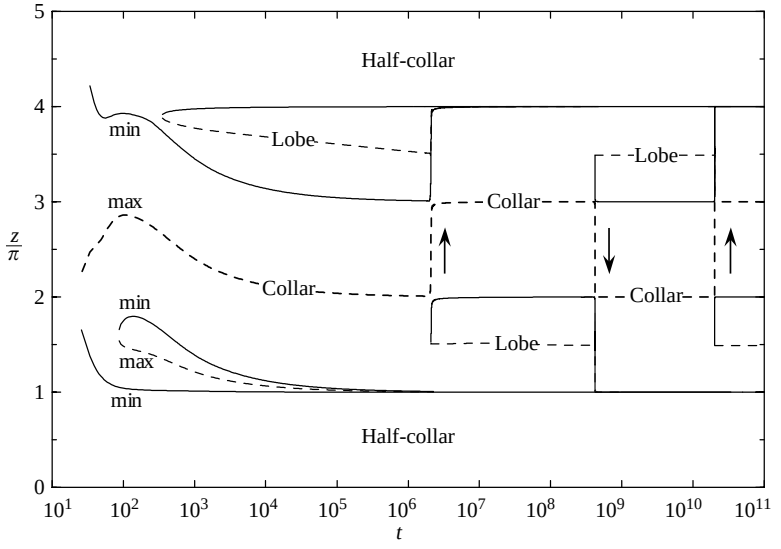

FIGURE 6. The locations of the main minima (solid) and maxima (dashed) for $L = 5\pi$ as functions of time (cf. figure 5). The central collar slides relatively rapidly between $1 < z/\pi < 3$ and $2 < z/\pi < 4$ at $t = 2 \times 10^6$, 4×10^8 and 2×10^{10} (arrows). The maxima at $z/\pi = 0$ and 5 remain stationary throughout; the maximum of the central collar oscillates to and fro between $z/\pi = 2$ and $z/\pi = 3$; the maximum of the lobe near $z/\pi = 1.5$ or 3.5 disappears abruptly when it is overrun by the central collar and reappears as a maximum of the daughter lobe on the other side of the collar.

recognizable half-collars at the ends of the domain, with a lobe in $1 < z/\pi < 2$ and a collar in $2 < z/\pi < 4$ (figure 1*a*). Subsequent snapshots of the film profile (figures 1 and 5) show that the collar and lobe swap places at least three times up to time $t = 10^{10}$ with the lobe becoming smaller on each occasion. The kinematics of these

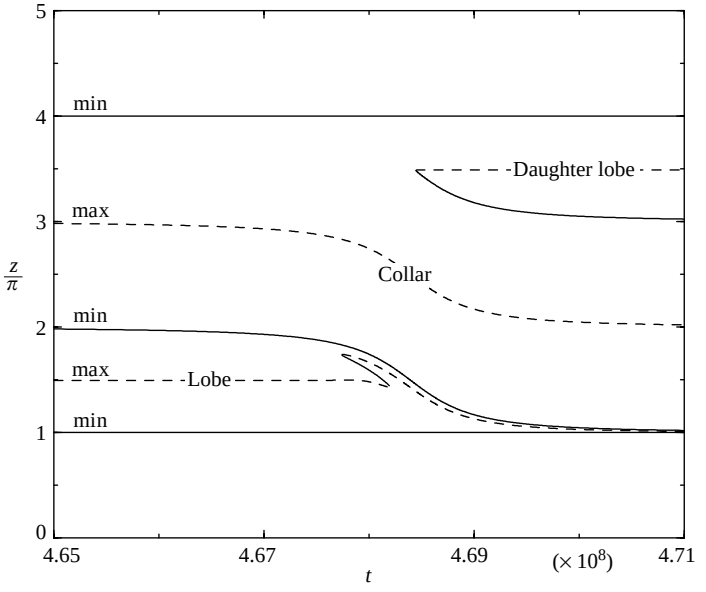

FIGURE 7. A detail of figure 6 expanded to show the sliding motion of the central collar near $t = 4.7 \times 10^8$ by the locations of the main minima (dashed) and maxima (solid). The lobe in $1 \leqslant z/\pi \leqslant 2$ is overrun by the sliding collar and a new daughter lobe is left behind in $3 \leqslant z/\pi \leqslant 4$.

swaps can be seen in figures 6 and 7. As t increases from 10^2 to 10^5 the collar slides to the left from $2 < z/\pi < 4$ into $1 < z/\pi < 3$, consuming the lobe ahead of it and leaving a smaller daughter lobe behind in $3 < z/\pi < 4$. At around $t = 2 \times 10^6$, the collar slides back to $2 < z/\pi < 4$ leaving an even smaller daughter lobe in $1 < z/\pi < 2$. The collar slides left again around $t = 4 \times 10^8$ (figure 7) and right again around $t = 2 \times 10^{10}$. Though each sliding event takes longer than the one before, the sliding time becomes negligible compared to the waiting time between sliding events and thus later sliding events appear to be instantaneous on the logarithmic timescale used. It can be seen from figure 5 that the amplitude of the lobe decreases by a factor of about 10 in each sliding event.

From figure 8 it can be seen that the amplitudes of the minima decrease like t^{-1} on average, though there are large perturbations during and after sliding. In contrast, after the early evolution the heights of the collars remain almost constant (figure 5) and the maximum height of the lobe is almost constant between sliding events (figure 8). The lobe height decreases in a stepwise fashion with an average rate of decrease consistent with a $t^{-1/2}$ power law. It can also be seen that there are two minima near one of the necks, either at $z/\pi = 1$ or $z/\pi = 4$, depending on which side of the domain the moving collar is at. The rate of dissipation Φ, evaluated using (2.8), also decreases episodically (figure 9) with large peaks during the sliding events.

Many of the details of these figures can be interpreted more fully in the light of the solutions to be developed in the following sections. It should be clear that in order to understand the physics of drainage at least three processes require description: the relatively rapid sliding of a collar across the domain; the slower t^{-1} decrease of the minima between adjacent, almost stationary collars; and the initiation of the next sliding event. These processes are the subjects of §§ 5–7.

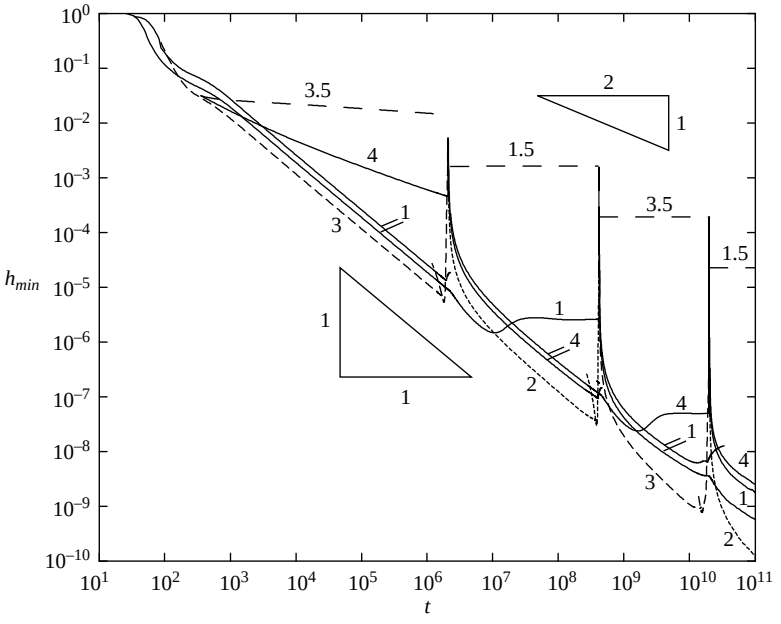

FIGURE 8. The heights of the main minima for $L = 5\pi$. The numbers denote the approximate value of z/π at the minima. A long-time average decrease proportional to t^{-1} can be seen for every minimum. The spikes correspond to rapid variations as the collar slides from one side to the other. The appearance of a secondary minimum near 2π or 3π just before each sliding event corresponds to the arrival of the peeling wave analysed in § 7. The long-dashed curves show the height of the lobe labelled by the approximate value of z/π at the maximum; the stepwise decrease is consistent with a very-long-time average proportional to $t^{-1/2}$.

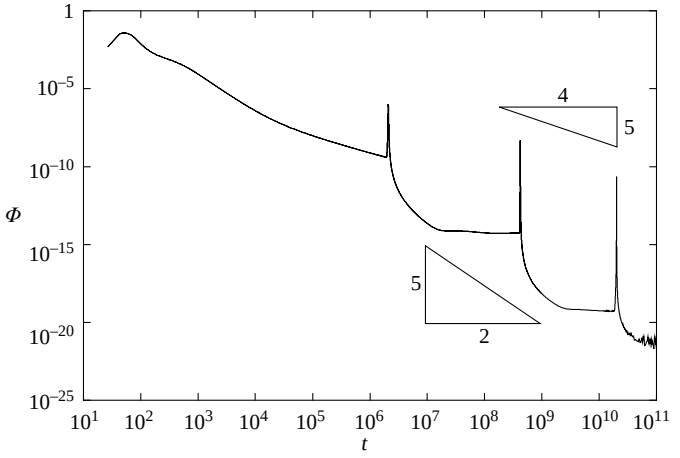

FIGURE 9. The rate of dissipation $\Phi = -\mathrm{d}E/\mathrm{d}t$ for $L = 5\pi$ as given by (2.8). The peaks occur during the sliding events and decrease roughly as $t^{-5/4}$. The decrease in Φ between two sliding events shows two regimes: first a rapid decrease that seems to tend towards $t^{-5/2}$; then a near-plateau region of very much slower decrease. These regimes correspond to the collision of collars and the peeling process analysed in §§ 6 and 7. The very-long-time average rate of decrease of Φ is consistent with $t^{-5/2}$. The features of this graph are discussed and interpreted further in § 7.3.

4. Interaction of two stationary collars, $L = 2\pi$

It is clear from figure 4 that for $L = 2\pi$ (and also for $L = 4\pi$) the heights of the minima between the adjacent collars decrease like t^{-1} instead of the Hammond scaling $t^{-1/2}$. These calculations represent something of a special case since the domain length is an integer multiple of the 2π length of a collar, but prove to be a useful step towards understanding the generic behaviour in longer domains when two collars collide. That the Hammond solution for an adjacent lobe and collar cannot describe the neck between adjacent collars can be seen from the fact that the similarity solution for (2.12) must match to a non-zero contact angle on one side.

A solution for the neck between two collars must match to prescribed $O(1)$ curvatures on either side. Since we have observed that $h \sim t^{-1}$, we thus expect the lengthscale of the neck to be $t^{-1/2}$. Accordingly, we seek an asymptotic solution of (2.5) in the similarity form

$$h(z,t) = t^{-1}F(\zeta), \quad \text{where} \quad \zeta = (z - z_n)t^{1/2} \tag{4.1}$$

and $z = z_n$ is the location of the neck. It follows that $h_z \ll h_{zzz}$ in the neck, so (2.5) reduces to the thin-film equation $h_t = \frac{1}{3}(h^3 h_{zzz})_z$, and F satisfies

$$-F + \tfrac{1}{2}\zeta F' + \tfrac{1}{3}(F^3 F''')' = 0. \tag{4.2}$$

The generic behaviour of (4.2) as $F \to \infty$ is given by $F''' \sim 0$ so that $F = \frac{1}{2}\alpha\zeta^2 + \beta\zeta + \gamma + O(\zeta^{-1})$, where α, β and γ are constants that may take different values on either side of the neck. We anticipate that four boundary conditions, obtained by matching the neck to the adjacent collars, will be needed to provide a unique solution to (4.2). The rescaling $F \to \lambda^4 F$, $\zeta \to \lambda^3\zeta$, where λ is a constant, leaves (4.2) invariant; solutions to (4.2) thus form a three-parameter family.

The similarity equation (4.2) is found to underpin most of the work in this paper. We will show in § 6 that in an appropriate asymptotic limit it includes the Landau–Levich equation (5.4) below. It is found also to describe the neck region between two colliding collars (with a double-minimum W-shaped solution) and the trailing edge of a colliding collar (with a single-minimum U-shaped solution). While this class of problem has received attention previously (Bertozzi *et al.* 1994; Hastings & Peletier 1998), we are not aware of any studies treating (4.2) subject to the boundary conditions we describe below.

For $L = 2\pi$ the two half-collars are pinned by the boundary conditions and take the form

$$h = A(1 + \cos z) + B, \tag{4.3}$$

with $A = A_-$ in $0 \leqslant z/\pi < 1$, $A = A_+$ in $1 < z/\pi \leqslant 2$ and $B = O(t^{-1})$. The values of $A_\pm$, which depend on the initial conditions, determine the quadratic coefficients α in the asymptotic behaviour of F as $\zeta \to \pm\infty$. For sideways translation of a collar with velocity $c(t)$, $h_t = -ch_z$. This condition can provide a consistent matching with a neck described by (4.1) and (4.2) only if $c = \beta t^{-3/2}/(2\alpha)$. Since for $L = 2\pi$ the half-collars are pinned with $c = 0$ by the boundary conditions at $z = 0,\ L$, we conclude that the linear terms must vanish and thus the appropriate boundary conditions for the similarity solution of (4.2) are

$$F = \tfrac{1}{2}A_\pm\zeta^2 + 0.\zeta + O(1) \quad \text{as} \quad \zeta \to \pm\infty. \tag{4.4}$$

Equations (4.2) and (4.4) were solved using MATLAB for $A_- = 1.523$ and $A_+ = 0.4766$. These values were chosen so as to correspond to the initial conditions (3.1) with $L = 2\pi$. Figure 10 shows excellent agreement with scaled profiles of the neck

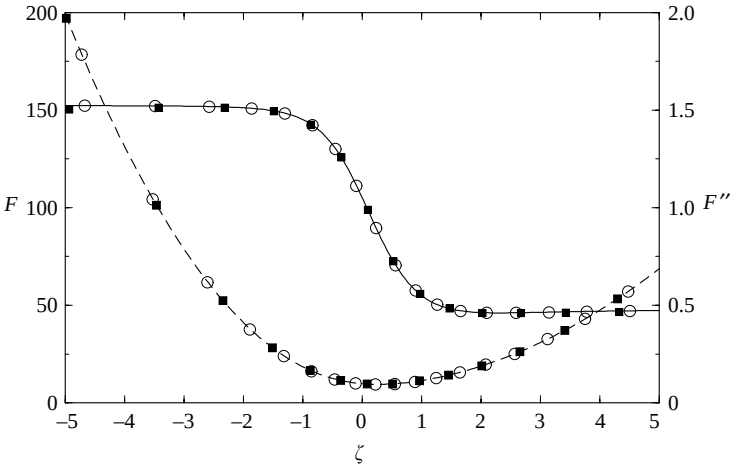

FIGURE 10. Solution of the similarity equations (4.2) and (4.4) for $A_- = 1.523$ and $A_+ = 0.4766$ showing F (dashed, left-hand scale) and F'' (solid, right-hand scale). Also shown are th and h_{zz} as functions of $\zeta = (z-\pi)t^{1/2}$ from the solution of (2.5) at $t = 10^4$ (squares, every 70th grid point) and $t = 10^8$ (circles, every 50th grid point).

at $z = \pi$ from the time-dependent solution of (2.5) at $t = 10^4$ and $t = 10^8$. Detailed examination of the time-dependent results shows that the term linear in ζ is indeed absent.

It is evident from (4.1) that the flux $q = \frac{1}{3}h^3 h_{zzz}$ in the neck scales as $t^{-5/2}$. Moreover, for stationary collars (4.2) shows that as $\zeta \to \infty$, $F \to \frac{1}{2}\alpha\zeta^2 + \gamma + O(\zeta^{-2})$ and thus $q \to \gamma\zeta t^{-5/2}$. Because this leading-order flux has opposite signs on either side of the neck, the conclusion in Jones & Wilson (1978) and Hammond (1983) that the flux is spatially uniform through the neck is not appropriate here: at leading order there is no net transfer of fluid from one collar to its neighbour (even though the associated pressures are different). Instead the flux arises principally because the neck thickness decreases in time and fluid is squeezed into the collars on either side at a rate proportional to $t^{-5/2}$. In consequence, the energetically favoured state in which one collar drains into its neighbour proves to be inaccessible: the neck collapses too rapidly.

The t^{-1} dependence of the neck thickness causes the values of A and B in (4.3) to vary slightly by $O(t^{-1})$ amounts. Thus in the collars, as in the neck, $h_t = O(t^{-2})$. Hence the flux q in the collar is $O(t^{-2})$. Since, as we have noted, the flux across $z/\pi = 1$ is $o(t^{-2})$, the volume of each collar is constant at leading order, and so $A_t \sim -B_t$ and $q \sim -(A_\pm)_t \sin z$. These conclusions are supported by plots of the scaled flux $t^2 q$ and $t^2 q_z$ in figure 11. The apparent jump in $t^2 q_z$ across $z/\pi = 1$, which is actually smoothed across the small $O(t^{-1/2})$ neck region, reflects the different values of γ as $\zeta \to \pm\infty$.

4.1. *The case* $L = 4\pi$

The case $L = 4\pi$ differs from $L = 2\pi$ in that the central collar is not quite stationary. After the initial translation to $1 < z/\pi < 3$ shown in figure 3(*d*), the collar is found numerically to drift sideways by an $O(t^{-1/2})$ distance with a speed $O(t^{-3/2})$. Equation (4.2) governs similarity solutions F_1 and F_3 for the necks near $z = \pi$ and $z = 3\pi$, but the drift velocity of the collar now requires a corresponding non-zero value of β on the appropriate side of each solution. Given β and the collar amplitudes, there are sufficient boundary conditions to determine F_1 and F_3; the value of β, and hence

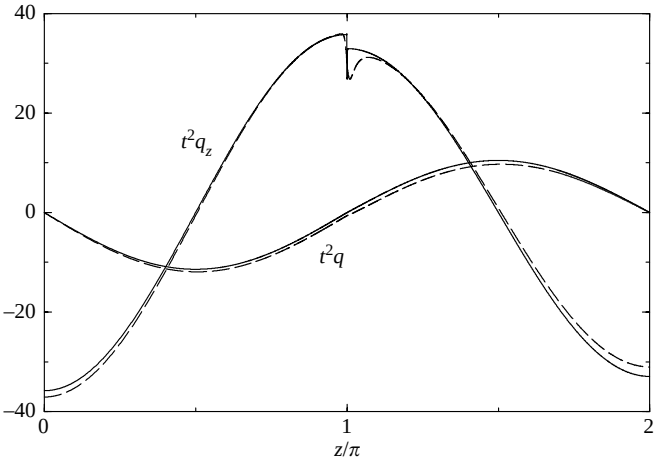

FIGURE 11. The scaled flux t^2q and t^2q_z for $L=2\pi$ from the solution of (2.5) at $t=10^4$ (dashed) and $t=10^8$ (solid). The flux across $z/\pi=1$ is $o(t^{-2})$. The form of q is consistent with $h_t \sim A_t \cos z$ in each collar.

the drift velocity, is determined by the additional matching condition that not only β but also γ is the same for F_1 as $\zeta \to \infty$ and for F_3 as $\zeta \to -\infty$. The above analysis of the central collar motion for the case $L=4\pi$ is extended to that of general collar collisions in § 6, and so we defer further discussion until then.

5. Sliding: translation of a collar over a lobe

From figures 5–7 it is evident that a collar with $h=O(1)$ can slide over a lobe with $h \ll 1$ leaving a new and even thinner lobe behind it. The process is readily understood once it is realized that a collar is capable of self-induced, surface-tension-driven translation over a uniform film. The analysis below is related to previous work (e.g. Kalliadasis & Chang 1994; Kerchman & Frenkel 1994; Chang & Demekhin 1999; Jensen 2000) on gravity-driven translation of a collar or drop along a tube or fibre, but shows that gravity is not necessary for translation; capillarity alone is sufficient provided some initial left–right asymmetry is present to start the motion off.

5.1. *Model problem*

We seek a solution of (2.5) that describes a collar of prescribed volume V of order unity translating with constant speed $c>0$ to be determined over a uniform (unstable) layer of much smaller prescribed thickness h_+. The translating collar leaves behind a layer of even smaller thickness h_- that we also wish to find. Under our non-dimensionalization, the speed c has the significance of a capillary number. The volume of the collar clearly increases at a rate $\mathrm{d}V/\mathrm{d}t = c(h_+ - h_-)$. From (2.11$a$, b) the energy of a collar is $-V^2/(4\pi)$, and the decrease of interfacial energy associated with the growth of the collar provides the driving force for translation.

Let $\delta=(h_+/A)^{1/2}$, where $A=V/2\pi$ is the amplitude of the collar, and suppose that $\delta \ll 1$. It follows that collar growth is slow over the time taken for propagation over its own length. We can thus look for a quasi-steadily propagating solution $h(z,t)=h(x)$, where $x=z-ct$, which satisfies

$$(h^3(h'+h'''))' = 3ch' + O(\delta^2 ch) \tag{5.1}$$

and $h \to h_\pm$ as $x \to \pm\infty$. In the collar $h = O(1)$ and $p = -h - h''$ is approximately constant. Anticipating the scaling $c = O(\delta^3)$, we can solve (5.1) to give the quasi-steady collar shape as

$$h = A(1 + \cos x) + B + O(\delta^3). \tag{5.2}$$

In order to match to the uniform films ahead and behind, we expect that $B = O(h_\pm) = O(\delta^2)$.

Near $x = \pm\pi$ there are small regions of size δ where the curvature changes rapidly in order to match the edges of the collar to the uniform films and hence $h''' \gg h'$. These regions are analogous to those in the Bretherton problem (Bretherton 1961). We rescale the variables accordingly, by defining

$$h = h_\pm H_\pm(\xi), \quad \text{where} \quad \xi = (3c)^{1/3}(x \mp \pi)/h_\pm. \tag{5.3a, b}$$

Integrating (5.1) once, we obtain at leading-order the Landau–Levich equation (Landau & Levich 1942)

$$H^3 H''' = H - 1 \tag{5.4}$$

in both regions. The neglected higher-order terms are $O(\delta)$. Equation (5.4) has a unique solution $H_-(\xi)$ with

$$H_- \to 1 \quad \text{as} \quad \xi \to -\infty, \qquad H_- \sim \tfrac{1}{2}a_-\xi^2 + b_- \quad \text{as} \quad \xi \to \infty, \tag{5.5a, b}$$

where $a_- = 0.6430$ and $b_- = 2.8996$ (e.g. Jensen 2000), and a one-parameter set of solutions $H_+(\xi;\lambda)$ labelled by λ with

$$H_+ \to 1 \quad \text{as} \quad \xi \to \infty, \qquad H_+ \sim \tfrac{1}{2}a_+(\lambda)\xi^2 + b_+(\lambda) \quad \text{as} \quad \xi \to -\infty. \tag{5.6a, b}$$

Matching (5.5*b*) and (5.6*b*) to (5.2), we find that

$$A(3c)^{-2/3} = a_-/h_- = a_+/h_+, \qquad B = h_-b_- = h_+b_+. \tag{5.7a, b}$$

It follows that $a_+(\lambda)b_+(\lambda) = a_-b_-$, which has a unique solution found numerically as $a_+ = 5.59$ and $b_+ = 0.333$, so that

$$h_- = (a_-/a_+)h_+ = 0.115h_+. \tag{5.8}$$

The propagation speed

$$c = \tfrac{1}{3}(Ah_+/a_+)^{3/2} = 0.646(Ah_-)^{3/2} \tag{5.9}$$

is $O(\delta^3)$ as expected.

There is a precursor capillary wave ahead of the collar where H_+ decays exponentially to unity. The e-folding decay length of this region is $[\frac{1}{2}(3c)^{1/3}/h_+]^{-1} \sim 5(h_+/A)^{1/2}$.

In order to test this analysis, we solved (2.5) numerically with initial condition

$$h = (1 + \cos\tilde{z}) + 0.009 + 0.001\sin(\tilde{z}/2) \quad (|\tilde{z}| \leqslant \pi), \tag{5.10a}$$

$$h = 0.009 + 0.001\,\mathrm{sgn}(\tilde{z}) \quad (|\tilde{z}| \geqslant \pi), \tag{5.10b}$$

where $\tilde{z} = z - 3\pi$. The value of δ is then 0.1. The difference in the initial thicknesses 0.008 and 0.01 on the two sides of the collar initiates motion to the right (figure 12), where the pressure is slightly lower, and after a short transient the collar is seen to undergo steady translation leaving a film of uniform thickness $h_- = 0.00124$ behind it. The capillary wave at the front of the collar agrees well with the predicted solution H_+ of (5.4). The 8 % difference may be attributable to $O(\delta)$ corrections. The numerics confirm that the speed of the steadily translating collar, and the thickness of the deposited film, are determined entirely by the amplitude of the collar and the

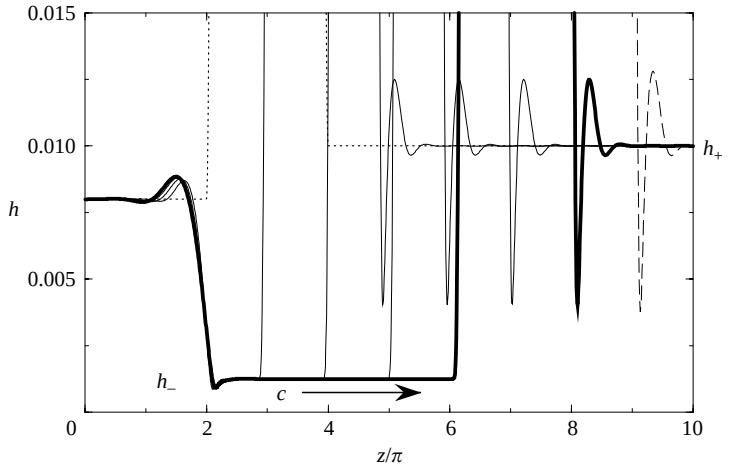

FIGURE 12. Quasi-steady translation of a collar with initial amplitude $A=1$ over a uniform layer with $h_+=0.01$. Most of the collar is thus off the vertical scale. The initial conditions (5.10) (dotted) describe a collar in $2<z/\pi<4$ with a film of thickness 0.008 in $z/\pi<2$ and 0.01 in $z/\pi>4$. As the collar slides to $6<z/\pi<8$ (bold) it deposits a film of thickness $h_-=0.00124$. The solutions (solid) are shown at equal time intervals of 10^5. The dashed curve is the leading-edge solution H_+ of (5.4) rescaled to give $h(x)$.

thickness of the film ahead of the collar (see (5.9)). Further analysis is required to describe the initial transient.

It is worth noting that the only assumption made in this analysis is that the amplitude of the collar is much larger than the lobe or layer thickness that it consumes. If the initial coating of the cylinder has thickness comparable to the cylinder radius then the equilibrium shape of a collar of large volume is determined by the condition of constant nonlinear curvature (2.1) and is non-sinusoidal. Nevertheless, provided the lobe or layer is sufficiently thin for (2.5) to apply, equation (5.8) for the thickness of the deposited layer still holds, but equation (5.9) for the speed of translation requires replacement of the factor A by the curvature at the foot of the finite-amplitude collar (see Gauglitz & Radke 1988; Jensen 2000; Lister *et al.* 2006).

5.2. *Application to the sliding collar*

The steady propagation speed in the model problem above is determined by the Landau–Levich regions at the edges of the collar, which have a short $O[(Ah_+)^{1/2}]$ lengthscale. It follows that if the film thickness in the lobe ahead of the collar varies on a much longer lengthscale then the collar should propagate quasi-steadily with a speed determined, using (5.9), by its amplitude A and the film thickness $h_+=h(z)$ just ahead of its leading edge. Similarly, from (5.8) the collar should deposit (for $c>0$) a daughter lobe of thickness $h_-(z)=0.115h(z+2\pi)$ behind it. Because the original lobe has constant curvature, so does the daughter lobe; thus no further adjustment of the daughter lobe is required in this regime.

The length of a lobe and the amplitude of a collar are generally $O(1)$ and thus the quasi-steady approximation should hold if the lobe thickness $h_+\ll 1$. The sliding collar in figure 7 has amplitude $A=1.285$, and the maximum thickness of the lobe being consumed is 0.00163, giving $\delta<0.04$. Figure 13 shows the speed of the collar maximum together with the speeds predicted from the lobe thicknesses h_+ and h_- by applying (5.9) and the quasi-steady approximation. The agreement is good, confirming not only the predicted time-dependence of the translation speed, but also the predicted

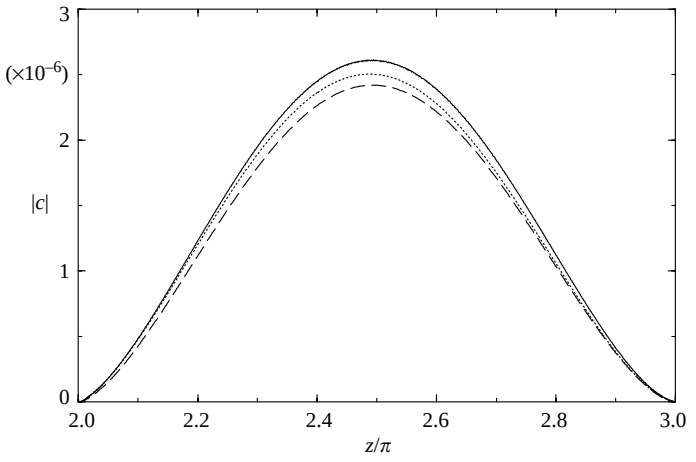

FIGURE 13. The speed $c<0$ of the collar maximum (solid) as a function of its position z for the sliding motion shown in figure 7. Also shown are the speeds predicted using (5.7*a*) from the computed shape h_+ of the lobe in $1<z/\pi<2$ at $t=4\times10^8$ (dashed) and from the computed shape h_- of the daughter lobe left in $3<z/\pi<4$ at $t=4.5\times10^8$ (dotted).

proportionality of the size of the original and daughter lobes. The small differences can again be attributed to the $O(\delta)$ corrections, including the variation of the initial lobe thickness over the scale of the Landau–Levich regions.

Taking the maximum height of the deposited daughter lobe as h_m, the time taken for a lobe of width π to be consumed may be estimated using (5.9) as $\pi/c=O[5(Ah_m)^{-3/2}]$. Thus the predicted duration of the sliding event at $t=2\times10^6$ in figure 6 (with $A\sim1$ and $h_m\sim10^{-3}$) is 2×10^5, and, on the assumption that drainage from the lobe is negligible between sliding events, each subsequent event takes a factor $(0.115)^{-3/2}\sim26$ longer, as may be seen in figure 7 for the next event.

As a collar of amplitude A approaches the far end of the lobe being consumed, both h_+ and c decrease toward zero. At distance Δz from the end of a lobe of length π, $h_+=O(4\Delta z\,h_m/0.115\pi)$ and so the length of the leading Landau–Levich region is, as estimated above after (5.9), $O[5(4\Delta z\,h_m/0.115\pi A)^{1/2}]$. By equating this length to Δz, we estimate that the regime of relatively rapid, quasi-steady sliding over a lobe finishes when $\Delta z=O(300h_m/A)$, $h_+=O(3000h_m^2/A)$ and $h_-=O(300h_m^2/A)$, and a new regime is entered in which the collar is almost, but not quite, stationary and adjacent to another collar. This new regime is long-lived and prevails during the long intervals between the relatively rapid sliding events (figure 6).

6. Stopping: the collision of two collars

The rapid sliding regime ends with the collision of the central sliding collar with the stationary half-collar at one end of the domain. In the new regime the central collar continues to move towards the end collar (figures 6, 7) with a velocity that is found to decrease like $t^{-3/2}$ (see below). Both the minimum height between the colliding collars and the minimum height between the moving collar and the trailing daughter lobe decrease like t^{-1} (figure 8). We now present analyses for the leading and trailing edges of the slowly moving collar. The analyses are good approximations, but are not ultimately asymptotic owing to the peeling process described in § 7 below that eventually ends the collision and initiates the next sliding event.

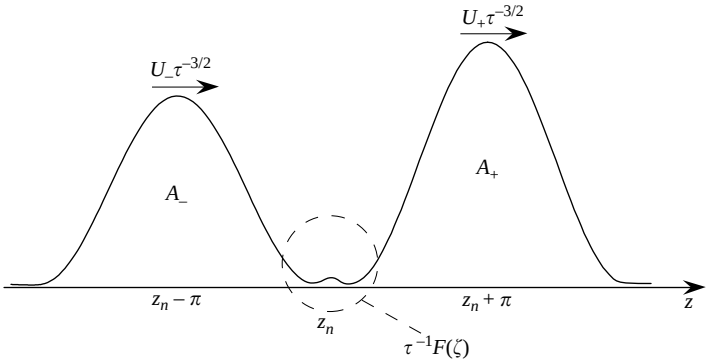

FIGURE 14. Schematic for the analysis in § 6.1. Collars with amplitudes $A_\pm$ and velocities $U_\pm\tau^{-3/2}$ collide. The solution near the collision at $z=z_n$ (detail) is described by a similarity solution of the form $h=\tau^{-1}F(\zeta)$ (see figure 15). For $L=5\pi$ either $U_-=0$ or $U_+=0$ owing to pinning of one collar by the boundary conditions.

6.1. *Leading edge of the colliding collar*

Motivated by the numerical results, we seek a similarity solution for colliding collars of the form

$$h(z,t)=\tau^{-1}F(\zeta), \quad \text{where} \quad \zeta=(z-z_n)\tau^{1/2}, \tag{6.1}$$

z_n is the location of the collision and $\tau=t-t_0$ is the time since the last sliding event at time t_0. The value of t_0 can only be defined approximately, but since the sliding event is relatively rapid, it may arbitrarily be taken as when the event is 90 % complete. As in § 4, F satisfies (4.2) and

$$F=\tfrac{1}{2}\alpha_\pm\zeta^2+\beta_\pm\zeta+\gamma_\pm+O(\zeta^{-1}) \quad \text{as} \quad \zeta\to\pm\infty. \tag{6.2}$$

The collars on either side of the collision are described by

$$h=A_\pm\left[1+\cos\left(z-z_n\mp\pi+2U_\pm\tau^{-1/2}\right)\right]+D_\pm\tau^{-1}, \tag{6.3}$$

where the collars move with velocities $c_\pm=U_\pm\tau^{-3/2}$ and the coefficients $D_\pm$ are $O(1)$ (figure 14). By matching the similarity solution to the collars, we deduce that the boundary conditions on (4.2) are now

$$F=\tfrac{1}{2}A_\pm\zeta^2+2A_\pm U_\pm\zeta+(2A_\pm U_\pm^2+D_\pm)+O(\zeta^{-1}) \quad \text{as} \quad \zeta\to\pm\infty. \tag{6.4}$$

The values of $A_\pm$ are given by the sizes of the collars and depend on the initial conditions. For $L=5\pi$ one of the collars is at the end of the domain and pinned by the boundary conditions; thus either $z_n=\pi$ and $U_-=0$ or $z_n=4\pi$ and $U_+=0$. An approximate theory for the velocity of the other collar will be discussed in § 6.3. For the moment, we use the numerically determined values $U_+=-20.3$ for $10^4<t<2\times10^6$ with $z_n=\pi$, and $U_-=24$ for $3\times10^6<t<4\times10^8$ with $z_n=4\pi$ (see figure 5). These values are estimated from the changes in position of the moving collar maximum and are subject to numerical uncertainties of ±2 % and ±5 % respectively. The four values $A_\pm, U_\pm$ provide the four boundary conditions in (6.4) needed to give a unique solution to (4.2).

In figure 15 we show five profiles from $10^4\leqslant t\leqslant10^6$ and five profiles from $3\times10^6\leqslant t\leqslant3\times10^8$, collapsed according to the similarity scaling (6.1). Also shown are the solutions of (4.2) with boundary conditions appropriate to the two time intervals. The agreement is excellent, showing that that the evolution of the neck is given by

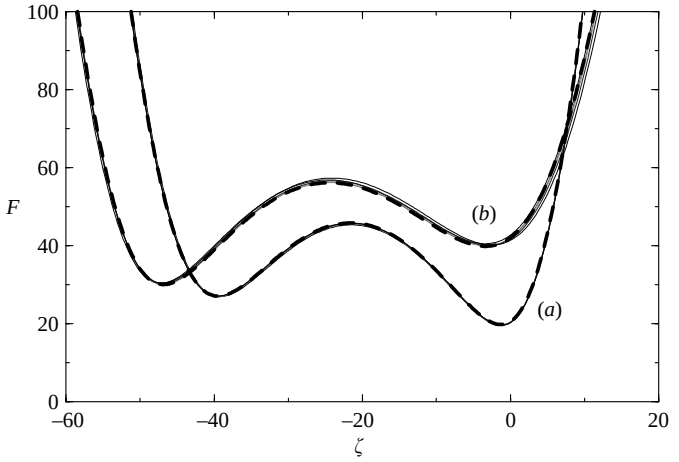

FIGURE 15. The shapes $h(z, t)$ (solid lines) scaled according to (6.1a) at various times together with the similarity solution (dashed) to (4.2) with boundary conditions (6.4). (a) The shapes at $t = 10^4$, 3×10^4, 10^5, 3×10^5 and 10^6 are plotted against $\zeta = (\pi - z)t^{1/2}$, and the similarity solution is for $A_- = 1.28$, $A_+ = 1.63$, $U_- = 20.3$ and $U_+ = 0$. (b) The shapes at $t = 3 \times 10^6$, 10^7, 3×10^7, 10^8 and 3×10^8 are plotted against $\zeta = (z - 4\pi)(t - 2.2 \times 10^6)^{1/2}$, and the similarity solution is for $A_- = 1.28$, $A_+ = 0.809$, $U_- = 24$ and $U_+ = 0$.

the similarity equations with the appropriate values of $A_\pm$ and $U_\pm$. The W-shapes correspond to the double minima seen in figure 8.

Some insight into the structure of the W-shaped solutions in figure 15 is provided by the following approximate analysis. Suppose the central hump, in $\zeta_- < \zeta < 0$, say, is approximately parabolic with maximum F_m, i.e. $F = 4F_m\zeta(\zeta_- - \zeta)/\zeta_-^2$. Then from (4.2) the scaled flux $Q = \frac{1}{3}F^3F'''$ satisfies $Q' = F - \frac{1}{2}\zeta F'$, which may be integrated to give $Q = Q_+ + F_m\zeta^2/\zeta_-$, where $Q_+ = Q(0)$. Let Q_- denote $Q(\zeta_-) = Q_+ + F_m\zeta_-$. Provided the values of F at the two minima are much smaller than F_m, the fluxes at the minima are approximately uniform and the Jones–Wilson solution (2.9) applies locally. Let $\theta = -4F_m/\zeta_-$ be the slope of the parabola at each end point. Then by setting $F = 3Q_+\theta^{-3}\mathscr{F}$ with $\zeta = 3Q_+\theta^{-4}\mathscr{X}$, and $F = 3Q_-\theta^{-3}\mathscr{F}$ with $\zeta - \zeta_- = -3Q_-\theta^{-4}\mathscr{X}$, we recover at each end the canonical problem

$$\mathscr{F}^3\mathscr{F}''' = 1, \quad \mathscr{F} \sim \tfrac{1}{2}\mathscr{C}\mathscr{X}^2 \text{ as } \mathscr{X} \to \infty, \quad \mathscr{F} \sim -\mathscr{X} \text{ as } \mathscr{X} \to -\infty, \tag{6.5}$$

with $\mathscr{C} \approx 1.2098$ (Jensen 1997), so that $q_\pm = \frac{1}{3}\mathscr{C}\theta^5/A_\pm$. Given the three parameters $A_\pm$ and U_- (with $U_+ = 0$) in (6.4), we now have sufficient conditions to determine $\zeta_- = -2U_-$, the fluxes $Q_+ > 0$ and $-Q_- < 0$ from the central hump to the right-hand and left-hand collars respectively and the hump maximum F_m. This approximation is asymptotic for solutions of (4.2) in which the values of F at its minima are much less than F_m and this is guaranteed whenever $U_-^{1/2}A_\pm^{3/4} \gg 1$. Even though the minimum values of F for the data in figure 15 are more than half of the maximum value, the composite approximation constructed by combining the parabolic outer and Jones–Wilson inner solutions in figure 16 (composite solutions for each half of the solution were patched together at $\zeta = \zeta_-/2$) captures the primary physical features of the solution reasonably well.

6.2. *Trailing edge of the colliding collar*

We have noted that when the collision occurs at the sliding collar's leading edge, the speed c of the collar ceases to be given by (5.9) and switches to $U\tau^{-3/2}$ for some

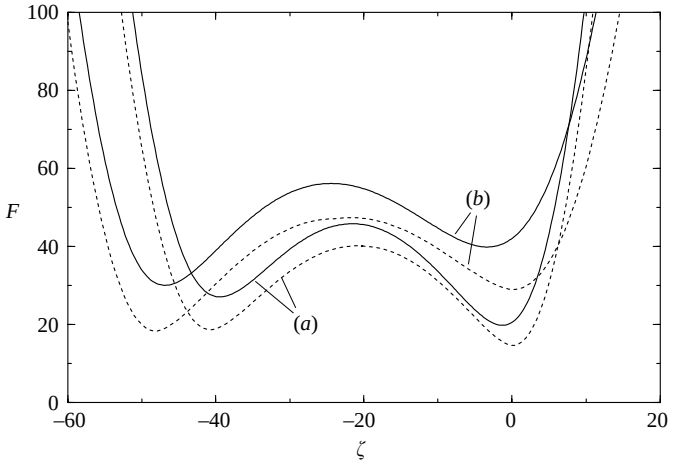

FIGURE 16. Similarity solutions (solid lines) from figure 15 together with composite approximations (dotted) based on patching Jones–Wilson inner solutions (6.5) for the minima to parabolic outer solutions. (*a*) $A_- = 1.28$, $A_+ = 1.63$, $U_- = 20.3$ and $U_+ = 0$. (*b*) $A_- = 1.28$, $A_+ = 0.809$, $U_- = 24$ and $U_+ = 0$.

U. Without loss of generality, we consider the case $U > 0$ so that the trailing edge is at $\tilde{x} = -2U\tau^{-1/2}$, where $\tilde{x} = z - (z_n - 2\pi)$. For the case $U < 0$ minor modifications are required to the direction of some of the limits. We also drop the subscript on the constants A and D that correspond to the shape of the moving collar in (6.3) since these constants describe the shape of the collar both ahead of its trailing edge and behind its leading edge. In this subsection the subscript '–' relates to the film deposited behind the trailing edge of the moving collar.

We assume, as a first approximation when U is large, that the collar motion continues to deposit a thin film quasi-steadily at the trailing edge with thickness h_- given by the Landau–Levich result in (5.7*a*). Thus the thickness deposited at $\tilde{x} = -2U\tau^{-1/2}$ is given by $Ah_- = a_-(3U)^{2/3}\tau^{-1}$. Eliminating τ, we obtain

$$h_- = \frac{3^{2/3}a_-\tilde{x}^2}{4AU^{4/3}} = 0.334\frac{\tilde{x}^2}{AU^{4/3}}. \tag{6.6}$$

From (5.3*b*) and (6.6), we deduce that the lengthscale of the Landau–Levich region is $O[\tilde{x}/(AU^{2/3})]$, which is short compared to $\tilde{x}$ provided $U \gg 1$. A crude estimate for U may be made by noting that the deposited film given by (6.6) must join on to the daughter lobe where $\tilde{x} \sim 300h_m/A$ and $h_- \sim 300h_m^2/A$. This gives $U \sim 20$; the measured numerical values are a little higher than this estimate. Although this lends weight to our suggestion that U may be treated as a numerically large parameter, we emphasize that U is not large in any asymptotic sense. Although the deposited layer (6.6) has constant curvature (of size about 0.01), this curvature differs, even in sign, from that of the main part of the daughter lobe. In consequence, its shape cannot persist for long times; some further adjustment in shape must take place. In figure 17 we show a series of profiles near the trailing edge of the collisions that occur during $10^4 \leqslant t \leqslant 2 \times 10^6$ and $3 \times 10^6 \leqslant t \leqslant 4 \times 10^8$. As the trailing edge approaches 2π and 3π, respectively, it can be seen that the collar does indeed deposit a film of thickness given approximately by (6.6). It can also be seen that the deposited quadratic profile is subsequently 'peeled' away again by a disturbance that follows and is catching up with the moving collar. This peeling wave is described further in § 7.

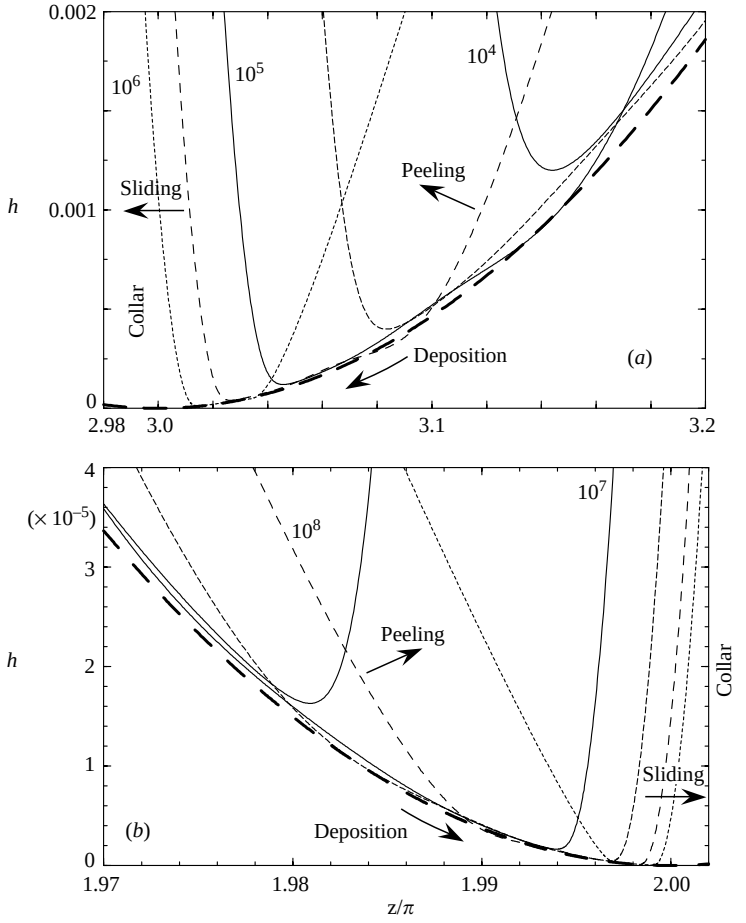

FIGURE 17. The neck shapes $h(z, t)$ at the trailing edge of the sliding collar at (*a*) $t = 10^4$, 3×10^4, 10^5, 3×10^5 and 10^6 and (*b*) $t = 3 \times 10^6$, 10^7, 3×10^7, 10^8 and 3×10^8. The quadratic profile (6.6) (long-dashed) gives an approximation to the film thickness deposited by the retreating collar, before it is peeled away again by the following disturbance. In (*a*) the collar is to the left and the daughter lobe, of height $h_m = 0.015$, is to the right; in (*b*) the collar is to the right and the daughter lobe, of height $h_m = 0.0016$, is to the left.

Because the deposited thickness varies like τ^{-1} over an $O(\tau^{-1/2})$ lengthscale, it is possible to replace the Landau–Levich approximation to the trailing-edge structure by another similarity solution of the form $h = \tau^{-1} F(\tilde{x}\tau^{1/2})$, where F satisfies (4.2) and boundary conditions of the form (6.4). Such a data collapse is shown in figure 18 for the deposition shown in figure 17(*a*). We note that the region of self-similar behaviour is of limited spatial extent, and further that it cannot describe the peeling event that follows: the peeling wave speed does not scale like $\tau^{-3/2}$ and hence the profile cannot be truly self-similar in the far field.

In order to determine the similarity function F, we suppose that a collar of specified amplitude A is sliding in the region $\zeta > 0$ with a known velocity $U\tau^{-3/2}$. The boundary conditions for (4.2) as $\zeta \to \infty$ are then $F \to \frac{1}{2}A\zeta^2 - 2UA\zeta + O(1)$. In addition, partly motivated by (6.6) and figure 18, we assume that as $\zeta \to -\infty$, $F \to \frac{1}{2}A_-\zeta^2 + O(1)$ for some A_-. Now with the change of variable $\tilde{\zeta} = \zeta - 2U$, the similarity equation (4.2)

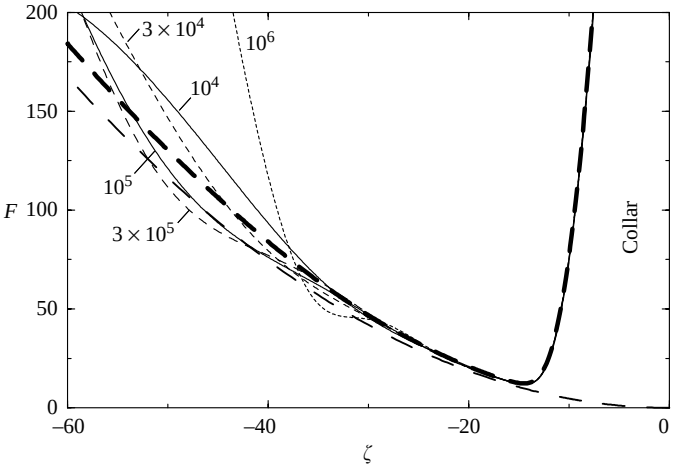

FIGURE 18. The five shapes from figure 17(*a*) replotted in similarity variables with $\zeta = (3\pi - z)t^{1/2}$. There is excellent collapse on the side of the retreating collar and near the minimum, but the peeling process disrupts self-similarity on the side of the deposited film. The quadratic profile (6.6) (long-dashed) slightly underestimates the deposited thickness. The similarity solution (6.7) (long-dashed, bold) with $U = 20.3$, $A = 1.28$ and A_- taken from (6.6) gives excellent agreement.

becomes

$$\frac{1}{3}\frac{\mathrm{d}}{\mathrm{d}\tilde{\zeta}}\left(F^3\frac{\mathrm{d}^3F}{\mathrm{d}\tilde{\zeta}^3}\right) = F - \frac{1}{2}\tilde{\zeta}\frac{\mathrm{d}F}{\mathrm{d}\tilde{\zeta}} + U\frac{\mathrm{d}F}{\mathrm{d}\tilde{\zeta}}, \tag{6.7}$$

which is computationally more convenient. Moreover, if $|U|$ is large the dominant balance is between the first and last terms, recovering the Landau–Levich equation (5.4) as the leading-order approximation, and suggesting that (6.6) may be used to give a first approximation for A_- as $0.668/AU^{4/3}$. Given the values of A and U, the similarity equation (4.2) or (6.7) then has a unique solution, which is plotted in figure 18 for $U = 20.3$ and $A = 1.28$; given the caveats expressed above, agreement with the collapsed data is remarkably good.

6.3. *Determination of the collision speed* $U\tau^{-3/2}$

We have shown that with a numerically fitted value for the collar speed $U\tau^{-3/2}$ it is possible, provided that $|U| \gg 1$, to explain the profile of h near the leading and trailing edges by means of the similarity equation (4.2). By combining these results we can find U to a good approximation.

The key is to match the constant $D\tau^{-1}$ for the shape (6.3) of the moving collar to the similarity solutions at the leading and trailing edges. For the leading edge, the coefficient γ_- in the expression (6.2) for the far field of F on the side of the moving collar may be found numerically from the similarity solution. The matching condition (6.4) gives $D = \gamma_- - 2AU^2$.

For the trailing edge of the moving collar, two levels of approximation are possible. If the trailing edge is treated as a Bretherton problem (appropriate in the limit $U \to \infty$) then from (5.5*b*) and (5.7), so that $D\tau^{-1} = b_-h_- = b_-a_-(3U)^{2/3}\tau^{-1}/A$, we deduce that

$$A\gamma_- - 2A^2U^2 = b_-a_-(3U)^{2/3}. \tag{6.8}$$

For the two collisions shown in figures 15 and 17, this equation gives $U = -15$ and $U = 18$ compared with the observed values $U = -20.3$ and $U = 24$ respectively.

An improved approximation is obtained by treating the trailing edge as a similarity equation as described in §6.2 above. In that case, as $\tilde{\zeta} \to \infty$, $F = \frac{1}{2}A\tilde{\zeta}^2 + \tilde{\gamma}$ for a constant $\tilde{\gamma}$ that is determined by the trailing-edge similarity solution and so

$$D = \tilde{\gamma} = \gamma_- - 2AU^2. \tag{6.9}$$

This equation, which now couples the behaviour at the leading and trailing edges, gives $U = -20.7$ and $U = 24.5$ for the two sliding events, in much closer agreement with the observed values.

We believe, but have not been able to prove, that this method provides the first two terms in an asymptotic expansion in $|U| \gg 1$; it seems fortuitous that the numerical value of $|U|$ is sufficiently large to provide good accuracy.

7. Peeling: adjustment of a daughter lobe

In our discussion of figures 17 and 18 we have already noted that the quadratic profile deposited by the trailing edge of a colliding collar is subsequently peeled away by a disturbance that follows the collar and eventually catches up with it. Peeling is the third and final process identified in § 3.2 to be understood.

7.1. *Model problem*

Peeling is driven by the difference in pressure between the daughter lobe created by sliding (§ 5.2) and the quadratic profile (6.6) created during collision (§ 6.2). It can be thought of as the daughter lobe spreading over the quadratic profile and adjusting toward a static equilibrium. Peeling is thus closely related to the simpler model problem of capillary spreading of a drop over a uniform precursor film.

As described by Tanner (1979) and Tuck & Schwartz (1990), capillary spreading over a uniform film can be analysed using another solution of the Landau–Levich equation (5.4) to describe the flow near the edge of the drop. We let the film thickness be h_0 and look for a travelling-wave solution to $3h_t + (h^3 h_{zzz})_z = 0$ with speed $c \ll 1$. On making the substitution

$$h = h_0 H(\xi), \quad \text{where} \quad \xi = (3c)^{1/3}(z - ct)/h_0, \tag{7.1}$$

and integrating once, we again obtain the Landau–Levich equation (5.4). In order to match to a uniform film ahead and the roughly linear profile of the edge of a capillary-static drop behind, we require

$$H \to 1 \quad \text{as} \quad \xi \to \infty, \qquad H = o(\xi^2) \quad \text{as} \quad \xi \to -\infty. \tag{7.2}$$

The absence of a quadratic term as $\xi \to \infty$ defines a unique solution ($a_- = 0$) among the one-parameter family $H_+(\xi\,;\lambda)$ of § 5.1. This solution obeys

$$H \sim -\xi(3\ln|\xi|)^{1/3} \quad \text{as} \quad \xi \to -\infty \tag{7.3}$$

and is shown in figure 19 with the origin chosen so $\xi = 0$ coincides with the pressure minimum. The minimum in H (≈ 0.82) corresponds to the secondary minimum that spontaneously appears in figure 8 just before each sliding event and that can be seen on the point of developing at $t = 10^6$ in figure 18.

If we match (7.3) to a drop with apparent contact angle $\theta = -h_z$ at height $h_\theta \gg h_0$ then we deduce that

$$c = \frac{\theta^3}{9\ln(h_\theta/h_0)} \tag{7.4}$$

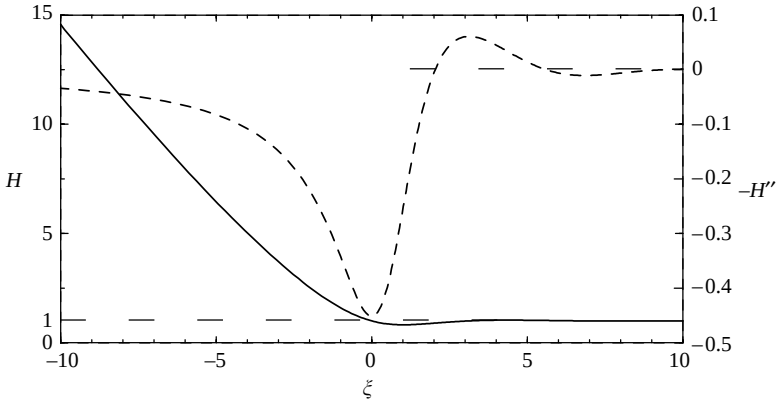

FIGURE 19. The solution to equations (5.4) and (7.2) for steady spreading over a film of uniform thickness: H (solid, left-hand scale); pressure $p = -H''$ (dashed, right-hand scale). The asymptotes $H \to 1$ and $H'' \to 0$ as $\xi \to \infty$ are shown long-dashed.

(cf. King & Bowen 2001), which is sometimes known as Tanner's law. A natural point for matching is the inflection point (Tanner 1979), where the positive pressure of the quasi-static drop is equal to the negative pressure in the outer limit of the Landau–Levich solution. Other prescriptions are formally equivalent to within the logarithmic errors involved in any leading-order approximation for this problem.

7.2. *Application to peeling near the trailing edge of a collar*

It may seem that Tanner's law applies to the peeling of the deposited layer in our full problem, using the inflection point of the daughter lobe to define the slope θ and the height h_θ. There are two difficulties with this direct application. First, the layer to be peeled has a quadratic thickness profile $h_-(\tilde{x})$ given by equation (6.6). Variations in layer thickness over the relevant Landau–Levich lengthscale $h_-/(3c)^{1/3}$ will be negligible only if $h'_-(\tilde{x}) \ll (3c)^{1/3}$ and, on the basis of the estimates made earlier, this requires that $\tilde{x} \ll 70h_m$. Second, the collar lies a distance at most $\tilde{x}$ ahead of the peeling wave, and this distance will only be large compared with the Landau–Levich lengthscale (so that the peeling wave does not 'see' the collar) if the same criterion $\tilde{x} \ll 70h_m$ is met. Thus, given that $\tilde{x} \sim 200h_m$ when peeling starts, Tanner's law can be expected to apply only late in the peeling process when the relevant value of h_- and the corresponding Landau–Levich lengthscale have decreased substantially. Paradoxically, this is close to the point at which the peeling wave catches up with the trailing edge of the collar so that peeling ceases! At earlier times, both the variations in the layer thickness and the proximity of the collar are likely to cause deviations from Tanner's law.

In order to facilitate comparison between the solution of the model problem and the peeling wave in the full problem, we rescale the numerical results in an analogous manner to (7.1). We define

$$H(\xi\,;t) = h(z,t)/h_p(t), \quad \text{where} \quad \xi = [3c(t)]^{1/3}[z - z_p(t)]/h_p(t), \tag{7.5}$$

$z_p(t)$ is the location of the pressure minimum of the peeling wave, $h_p(t) = h(z_p, t)$ and $c(t) = \mathrm{d}z_p/\mathrm{d}t$. The resultant pressure profiles at various times are shown in figure 20.

The scaling (7.5) successfully collapses the width of the main pressure minimum, but not its amplitude, and reproduces the form of the pressure profile (figure 19) for steady spreading on the peeled side ($\xi < 0$). The lack of collapse in $\xi > 3$ reflects the

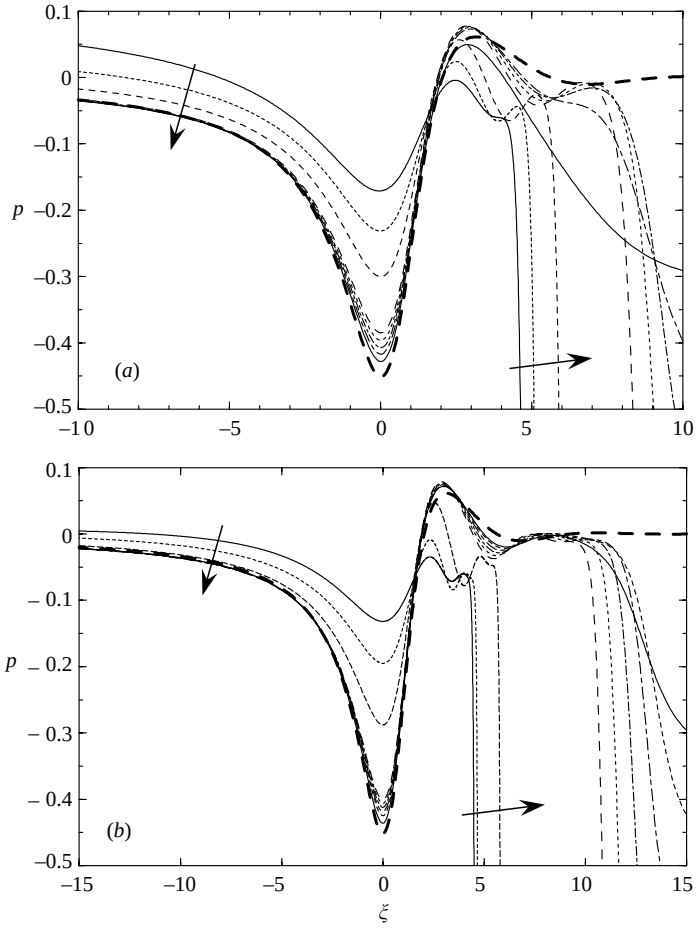

FIGURE 20. The pressure in the peeling wave for two different sliding events at various times rescaled according to (7.5). The profiles approach the solution (bold, long-dashed) for steady spreading over a precursor film of uniform thickness. (*a*) $t = 3 \times 10^4$, 10^5, 3×10^5, 10^6, and 1.2, 1.4, 1.6, 1.8×10^6. (*b*) $t = 10^7$, 3×10^7, 10^8, and 3.0, 3.2, 3.4, 3.6, 3.8×10^8. Arrows show increasing times.

fact that the neighbouring collar, with its large negative pressures, is sufficiently close to be seen on this scale. As t increases towards 2×10^6 and 4×10^8, the amplitudes of the main pressure minimum and the maximum near $\xi = 3$ approach those for steady spreading. This is probably due to the fact that the height h_p, which is part of the lengthscale used to define ξ, is decreasing like t^{-1}, more rapidly than the distance (in z) between the peeling wave and the collar, and hence the collar is becoming more distant in ξ. The peeling wave is, however, catching up with the trailing edge of the collar in the original coordinate z.

In figure 21 we compare the speed $\mathrm{d}z_p/\mathrm{d}t$ of the peeling wave to the Tanner-law prediction (7.4), where $\theta(t)$ and $h_\theta(t)$ are defined from the slope and height at the inflection point in the numerical profiles. The decrease with time in the predicted speed is largely due to the decrease of $h_p(t)$ and the consequent increase of the logarithm in (7.4). We have been unable to find a convincing physical explanation for the extent of the substantial under-prediction of the actual peeling speed at early times: the

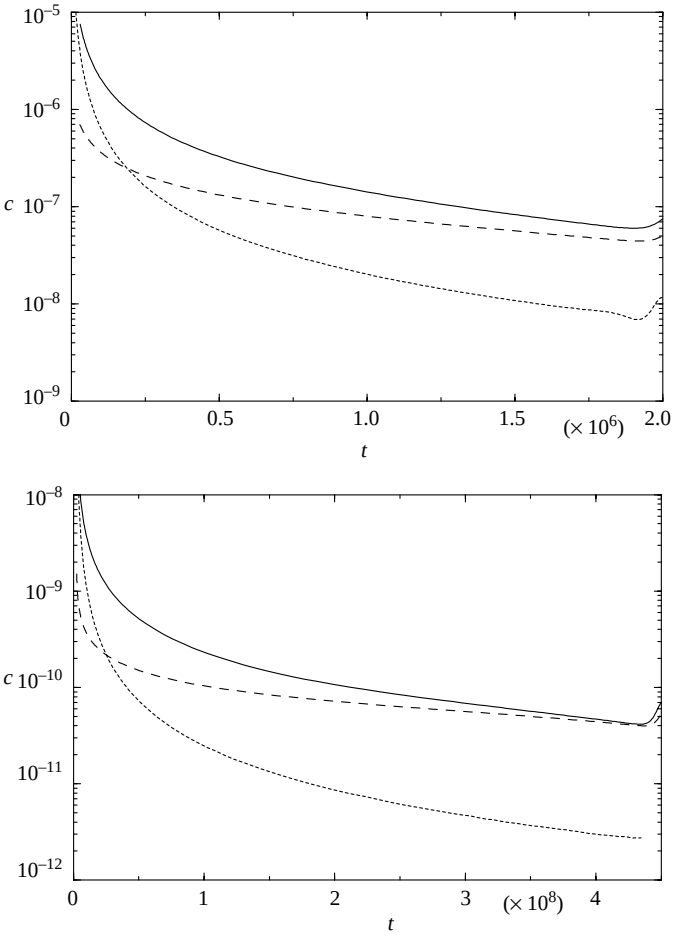

FIGURE 21. The speeds of the pressure minimum in the peeling wave (solid) and of the collar (dotted). The peeling-wave speed is increasingly well predicted by (7.4) (dashed line) and is sufficiently large for the peeling wave to catch up with the trailing edge of the collar in finite time.

flux from the nearby collar is negligible, and separate numerical calculations show that it is reasonable to use (7.4) as a quasi-steady approximation for spreading over a non-uniform layer. The improving agreement as t increases mirrors that of the pressure profiles in figure 20, and suggests that the issue may again be the distance to the collar on the scale of ξ. It is striking that the variation in velocity with time appears similar in form for the two sliding events in figure 21, apparently scaling as h_m^3 and thus differing in magnitude by a factor 0.115^3. This observation hints at an unexplained universal behaviour.

The figure also shows that the speed of the peeling wave is significantly greater than the speed of the centre of the collar ahead. As a result, the peeling wave catches up with the collar in a finite time, triggering a sudden increase in the thickness of the minimum between the lobe and the collar (cf. figure 8). The thickness at the trailing edge of the collar now exceeds that at the leading edge and the collar motion reverses, sliding rapidly back over the daughter lobe by the mechanism of § 5 leaving a new and smaller grand-daughter lobe on the other side.

7.3. *Timescale between sliding events, the long-term evolution of lobes and energy*

The timescale for the increasingly long intervals between successive sliding events is dominated by the time taken for the peeling wave to catch up with the decelerating collar. As argued in § 5.2, the collar velocity decreases rapidly like $\tau^{-3/2}$ after the collision begins at a distance $\Delta z = O(200h_m)$ from the next collar. If we assume that the peeling wave must also travel this distance to catch up with the collar and that the peeling-wave speed scales as h_m^3 then the interval between sliding events is $O(h_m^{-2})$. Since h_m decreases by a factor 0.115 during each event, we expect the peeling-wave speed to decrease by a factor of about 10^{-3} and the interval between events to increase by a factor of about 10^2. These conclusions are approximately borne out by figure 21 and the intervals between the events in figure 6. We note that the durations of successive sliding events are not exactly the same owing to the difference between the amplitudes of the two half-collars at the ends of the domain.

Furthermore, the decrease of h_m by a factor 10^{-1} in events separated by a factor 10^2 in time suggests that the lobe height $h_m(t)$ decreases episodically at an average rate proportional to $t^{-1/2}$ consistent with the long-dashed line in figure 8. This decrease is more rapid than the $t^{-1/4}$ prediction for a lobe next to a stationary collar (Hammond 1983). We enter a caveat however. The appearance of logarithmic terms in (7.4) cautions that the peeling-wave speed may differ from $O(h_m^3)$ by a logarithmic factor, in which case the scaling for the average rate of decrease of h_m may also need modification by a logarithmic factor. We do not have sufficient numerical data to distinguish a correction of this kind.

The above scaling for h_m also provides an explanation of the major variations of the rate of dissipation with time in figure 9. The dissipation occurs predominantly in the short regions at the edges of collars, where $h_{zzz} \gg h_z$. Thus $\Phi = O(\bar{h}^5/\bar{z}^5)$, where $\bar{h}$ and $\bar{z}$ are the typical scales of h and z in these regions. During sliding, $\bar{h} \sim h_m$ and $\bar{z} \sim h_m^{1/2}$ (§ 5.2) so that the episodic decrease of h_m like $t^{-1/2}$ gives a decrease in the peak values of Φ like $t^{-5/4}$. The similarity form $\bar{h} \sim t^{-1}$ and $\bar{z} \sim t^{-1/2}$ of (6.1) gives $\Phi \sim t^{-5/2}$ during the early stage of collisions. During the later stage of collisions, the dominant dissipation is associated with peeling for which $\bar{h}/\bar{z}$ scales with the peeling angle θ, where $\theta \propto h_m$. Thus $\Phi \propto h_m^5$ is approximately constant during each peeling event, but decreases by a factor 10^5 between events and like $t^{-5/2}$ on a long-term average. Finally, we note that the decrease in the energy E is dominated by the sliding events during which an $O(h_m^{5/2})$ dissipation rate acts for an $O(h_m^{-3/2})$ time to produce an $O(h_m)$ decrease in energy by transfer of fluid from the consumed lobe to the sliding collar. In the numerical calculations for $L = 5\pi$ (figure 9) the energy decreases from an initial value $E_0 = -7.9$ corresponding to (3.1) to a final value $E_\infty = -10.4$ corresponding to two half-collars and a collar with amplitudes $A = 1.63$, 0.81 and 1.28 respectively. The minimum-energy configuration comprising a single collar with $V = 5\pi$ and $E = -19.6$ is never attained.

8. Collar dynamics in a larger domain

As we have seen in § 3.2, the evolution on short domains ($L \leqslant 4\pi$) is geometrically constrained by the boundary conditions and hence is very much simpler than the evolution on a domain of length $L = 5\pi$, where there is sufficient room for the single central collar to move. For $L = 5\pi$ the interaction of sliding, stopping and peeling, analysed in §§ 5–7, gives rise to the complex dynamics seen in figures 5–8. It is natural to ask whether new phenomena appear in the dynamics when $L > 6\pi$ and there is room for two or more collars to move in the central region.

Preliminary numerical investigations on such longer domains suggest that this is not the case and that the dynamics can be decomposed into a sequence of the sliding, stopping and peeling processes already discussed for a single moving collar. In particular, it appears that generically collars slide over lobes one at a time and not in linked trains. Two collars brought together by a collision may remain together for a while in the almost-stationary regime of § 6, but separate as soon as one of them starts to slide. A heuristic explanation is that when one collar starts to slide away it leaves a thinner film behind it and the other collar will either slide more slowly on this thinner film and thus get left behind or, more likely, be triggered into sliding in the other direction (cf. the initial conditions in figure 12).

The number of collars, their sizes and locations, the exact sequence of collar motions, which collars collide with each other and when, all depend strongly on the length of the domain and the initial conditions, but the following general principles apply even to long domains. First, a collar, once formed, retains its identity; the number of collars never decreases in time. Second, collars move individually rather than in trains. Third, a collar will occasionally slide over a lobe in such circumstances as to bring two lobes together. These lobes then merge, forming a new collar whenever their joint length exceeds 2π. Thus there is a gradual reduction in the total number of lobes. An exhaustive investigation leading to a statistical description of the motion of many collars is, however, beyond the scope of this paper.

9. Discussion

We have shown in this paper that the evolution of a thin annular film depends, both qualitatively and quantitatively, on its length. For short lengths the evolution is well-described by the theory of stationary collars and lobes considered by Hammond (1983). But for greater lengths, collars do not remain stationary and several new phenomena involving the sliding and collision of collars and the peeling of lobes arise. A striking feature of the nonlinear dynamics is the wide disparity in timescales that appear. With an initial layer thickness $\hat{h}$, the time taken for formation of the initial collar and lobe structure is $\hat{t} = \mu a^4/\sigma \hat{h}^3$. Collars continue to have a typical height $\hat{h}$ subsequently and so adjust their shape on the timescale $\hat{t}$. Lobes, however, episodically lose volume when a collar slides over them so that the lobe height becomes $h_m(t)\hat{h}$. The time taken for a sliding event scales as $h_m^{-3/2}\hat{t} \gg \hat{t}$. The time taken for the subsequent peeling process when the collar is almost stationary is much longer, scaling as $h_m^{-2}\hat{t}$.

A somewhat disappointing feature of our results is that, for the initial conditions chosen, the first clear-cut example of peeling triggering a sliding event only occurs after a time $10^6\hat{t}$ for which the minimum film thickness has fallen to $10^{-5}\hat{h}$; for experimentally plausible parameter values, this thickness is so small as probably to be influenced by van der Waals forces or surface roughness. On the other hand, there is a clear example of sliding over the period $10^2\hat{t}$ to $10^5\hat{t}$ (figure 5); thus for times as small as $10^2\hat{t}$ we predict a noticeable axial drift of collars in sufficiently long domains and this drift should be accessible to experimental observation. We are not aware of any such observations at the present time.

It is interesting to contrast the sliding of a collar under the action of viscous and capillary forces alone (§ 5) with that of a droplet in equilibrium with a neighbouring ultra-thin film in the presence of capillary forces and short-range-repulsive, long-range-attractive intermolecular forces. Glasner & Witelski (2003) show how, in the latter case, there is a linear pressure gradient across the film between adjacent drops,

and that each drop moves in response to the weak fluxes driven by differing pressure gradients in the films on either side of the drop. In this case the drop is under edge control, with the conditions at the front and rear of the drop being of equal importance. The energy required to sustain the motion is released by transfer of fluid from the smaller to the larger drops. A collar also moves along a cylindrical film under edge control (§ 5), but it quickly adopts a quasi-steady configuration in which only conditions at the leading edge are significant. The energy required to sustain the motion is released in this case by transfer of fluid from the film to the collar and a reduction in film thickness. A much more profound difference occurs at long times: if film thicknesses are bounded away from zero by intermolecular forces then coarsening of multiple drops can occur by coalescence (Glasner & Witelski 2003); when there is no such constraint, severe thinning of the film between neighbouring collars provides a dissipative barrier to coalescence that inhibits long-time coarsening.

Weak gravity acting over long times can have a significant effect, so that the limit of zero Bond number is often singular. We have recently shown (King 2005) that, for a liquid-lined horizontal cylinder, weak gravity acts as a regular perturbation to a collar, whereas it acts as a singular perturbation to an axially uniform film by causing it to drain until it is pinned at contact lines at the top of the cylinder (Jensen 1997). Since collars preserve their identity, it is tempting to speculate that the picture described in this paper is broadly preserved in the presence of weak gravity acting normal to the cylinder axis. The situation for a vertical cylinder in the presence of weak gravity is less obvious. Gravity causes collars to drift downwards, with larger collars travelling faster than smaller ones, and collars can grow to finite amplitude in finite time provided they are well separated (Kalliadasis & Chang 1994; Jensen 2000). A small gravitational term added to (2.5) is thus not just singular, it may actually make the problem exhibit finite-time blow-up for certain initial conditions on an infinite domain. While the film thickness is much larger than $O(\Delta\rho\, g a^3/\sigma)$, the flow is dominated by the surface-tension effects described herein. Exploratory calculations on a periodic domain show that, as the lobe thickness decreases towards this order of magnitude, the episodic surface-tension-driven sliding gives way to a steady gravitationally driven downward drift of collars, which leaves a uniform film thickness equal to the critical value $1.68\Delta\rho\, g a^3/\sigma$ identified by Kalliadasis & Chang (1994). It thus seems that even a very small gravitational forcing along the axis will ultimately disrupt the long-time dynamics described here.

Though collar motion in the presence of axial forcing such as gravity, an axial temperature gradient (Wilson 1995) or axial variation in the cylinder radius (Lorenceau & Quéré 2004) is to be expected, it was at first surprising to find self-sustained axial motion of a single collar under the influence of surface tension alone. The driving mechanism, the difference between leading and trailing film thicknesses and the consequent net transfer of fluid from the film to the collar, appears to be robust. We speculate that this mechanism may contribute to the axial motion of curtains and ribs in some regimes of the rotating coated cylinder experiment (Moffatt 1977). Calculations to be presented elsewhere show that this mechanism can drive sustained lateral motion of a pendent drop over a horizontal liquid layer coating the underside of a ceiling. Preliminary numerical calculations show that the additional freedom allowed by lateral motion in two dimensions leads to complicated collisional dynamics between two such translating drops.

A. A. K. was supported by the EPSRC. L. J. C. thanks the National Grid for financial support in the form of a Royal Society Dorothy Hodgkin Fellowship.

Appendix. Numerical discretization

Let $h_i^j = h(x_i, t_j)$ denote the discrete representation of the film thickness on an arbitrarily spaced grid $x_0 = 0, \ldots, x_N = L$ at time t_j. The symmetry boundary conditions (2.6) are implemented by extending the grid by two points at either end and assigning the appropriate mirror values. The pressure at the grid points is approximated by

$$p_i^j = u_i h_{i-1}^j + (1 - u_i - v_i) h_i^j + v_i h_{i+1}^j, \tag{A 1}$$

where

$$u_i = \frac{2}{(x_i - x_{i-1})(x_{i+1} - x_{i-1})}, \qquad v_i = \frac{2}{(x_{i+1} - x_i)(x_{i+1} - x_{i-1})}. \tag{A 2}$$

Equation (2.5) is then represented by

$$3\frac{h_i^{j+1} - h_i^j}{t_{j+1} - t_j} = u_i c_{i-\frac{1}{2}} \left(p_{i-1}^{j+1} - p_i^{j+1}\right) + v_i c_{i+\frac{1}{2}} \left(p_{i+1}^{j+1} - p_i^{j+1}\right), \tag{A 3}$$

where $2c_{i\pm\frac{1}{2}} = (h_i^j)^3 + (h_{i\pm1}^j)^3$. Equation (A 3) is a linear pentadiagonal system of equations for the new thicknesses h_i^{j+1}, which gives second-order accuracy in space and first-order in time. Time steps were chosen conservatively such that h did not change by more than 0.2 % at any point. Spatial resolution was maintained by adding and redistributing points to maintain a grid density proportional to $1 + h^{-1/2}$. Tests using twice the density of grid points or half the timestep gave results that could barely be distinguished in the plots shown, with the exception that the time of later sliding events was changed by about 10 %, due perhaps to a slightly different early evolution. Further indications of resolution and accuracy, especially in the thin necks, are provided by the agreement between the time-dependent simulations and the similarity solutions in figures 10 and 15.

REFERENCES

Allen, J. S. & Hallinan, K. P. 2001 Liquid blockage of vapor transport lines in low Bond number systems due to capillary-driven flows in condensed annular films. *Intl J. Heat Mass Transfer* **44**, 3931–3940.

Ascoli, E. P., Dandy, D. S. & Leal, L. G. 1990 Buoyancy-driven motion of a deformable drop toward a planar wall at low Reynolds number. *J. Fluid Mech.* **213**, 287–311.

Aul, R. W. & Olbricht, W. L. 1990 Stability of a thin annular film in pressure-driven, low-reynolds-number flow through a capillary. *J. Fluid Mech.* **215**, 585–599.

Bertozzi, A. L., Brenner, M. P., Dupont, T. F. & Kadanoff, L. P. 1994 Singularities and similarities in interface flows. In *Trends and Perspectives in Applied Mathematics* (ed. L. Sirovich). Springer.

Bertozzi, A. L., Grun, G. & Witelski, T. P. 2001 Dewetting films: bifurcations and concentrations. *Nonlinearity* **14**, 1569–1592.

Bertozzi, A. L. & Pugh, M. C. 1998 Long-wave instabilities and saturation in thin film equations. *Commun. Pure Appl. Maths* **51**, 625–661.

Braun, R. J. & Fitt, A. D. 2003 Modelling drainage of the precorneal tear film after a blink. *Math. Med. Biol.* **20**, 1–28.

Bretherton, F. P. 1961 The motion of long bubbles in tubes. *J. Fluid Mech.* **10**, 166–188.

de Bruyn, J. R. 1997 Crossover between surface tension and gravity-driven instabilities of a thin fluid layer on a horizontal cylinder. *Phys. Fluids* **9**, 1599–1605.

Chang, H.-C. & Demekhin, E. A. 1999 Mechanism for drop formation on a coated vertical fibre. *J. Fluid Mech.* **380**, 233–255.

Everett, D. H. & Haynes, J. M. 1972 Model studies of capillary condensation 1. Cylindrical pore model with zero contact angle. *J. Colloid Interface Sci.* **38**, 125–137.

Fermigier, M., Limat, L., Wesfreid, J. E., Boudinet, P. & Quilliet, C. 1992 Two-dimensional patterns in Rayleigh-Taylor instability of a thin-layer. *J. Fluid Mech.* **236**, 349–383.

Frenkel, A. L., Babchin, A. J., Levich B. G., Shlang T. & Sivashinsky, G. I. 1987 Annular flows can keep unstable films from breakup — nonlinear saturation of capillary instability. *J. Colloid Interface Sci.* **115**, 225–233.

Gauglitz, P. A. & Radke, C. J. 1988 An extended evolution equation for liquid-film break up in cylindrical capillaries. *Chem. Engng Sci.* **43**, 1457–1465.

Glasner, K. B. & Witelski, T. P. 2003 Coarsening dynamics of dewetting films. *Phys. Rev.* E **67**, 016302.

Goren, S. L. 1962 The instability of an annular thread of fluid. *J. Fluid Mech.* **12**, 309–319.

Grotberg, J. B. & Jensen, O. E. 2004 Biofluid mechanics in flexible tubes. *Annu. Rev. Fluid Mech.* **36**, 121–147.

Hagedorn, J. G., Martys, N. S. & Douglas, J. F. 2004 Breakup of a fluid thread in a confined geometry: droplet-plug transition, perturbation sensitivity, and kinetic stabilization with confinement. *Phys. Rev.* E **69**, 056312.

Halpern, D. & Grotberg, J. B. 2003 Nonlinear saturation of the Rayleigh instability due to oscillatory flow in a liquid-lined tube. *J. Fluid Mech.* **492**, 251–270.

Hammond, P. S. 1983 Nonlinear adjustment of a thin annular film of viscous fluid surrounding a thread of another within a circular cylindrical tube. *J. Fluid Mech.* **137**, 363–384.

Hastings, S. P. & Peletier, L. A. 1998 On the self-similar solutions of the thin film equation when $n = 3$. *Diffl Integral Equat.* **11**, 1–22.

Hosoi, A. E. & Mahadevan, L. 1999 Axial instability of a free-surface front in a partially filled horizontal rotating cylinder. *Phys. Fluids* **11**, 97–106.

Jensen, O. E. 1997 The thin liquid lining of a weakly curved cylindrical tube. *J. Fluid Mech.* **331**, 373–403.

Jensen, O. E. 2000 Draining collars and lenses in liquid-lined vertical tubes. *J. Colloid Interface Sci.* **221**, 38–49.

Jensen, O. E., Chini, G. P. & King, J. R. 2004 Thin-film flows near isolated humps and interior corners. *J. Engng Maths* **50**, 289–309.

Johnson, M., Kamm, R. D., Ho L. W., Shapiro A. & Pedley, T. J. 1991 The nonlinear growth of surface-tension-driven instabilities of a thin annular film. *J. Fluid Mech.* **233** 141–156.

Jones, A. F. & Wilson, S. D. R. 1978 The film drainage problem in droplet coalescence. *J. Fluid Mech.* **87**, 263–288.

Joseph, D. D., Bai, R., Chen, K. P. & Renardy, Y. Y. 1997 Core-annular flows *Annu. Rev. Fluid Mech.* **29**, 65–90.

Kalliadasis, S. & Chang, H.-C. 1994 Drop formation during coating of vertical fibres. *J. Fluid Mech.* **261**, 135–168.

Kerchman, V. 1995 Strongly nonlinear interfacial dynamics in core–annular flows. *J. Fluid Mech.* **290**, 131–166.

Kerchman, V. I. & Frenkel, A. L. 1994 Interactions of coherent structures in a film flow: simulations of a highly nonlinear evolution equation. *Theor. Comput. Fluid Dyn.* **6**, 235–254.

King, A. A. 2005 The effects of surface tension and gravity on a liquid film lining a tube. PhD dissertation, University of Nottingham.

King, J. R. & Bowen, M. 2001 Moving boundary problems and non-uniqueness for the thin film equation. *Eur. J. Appl. Maths* **12**, 321–356.

Kliakhandler, I. L., Davis, S. H. & Bankoff, S. G. 2001 Viscous beads on vertical fibre. *J. Fluid Mech.* **429**, 381–390.

Landau, L. D. & Levich, B. 1942 Dragging of a liquid by a moving plate. *Acta Physicochim. URSS* **17**, 42–54.

Limary, R. & Green, P. F. 2003 Dynamics of droplets on the surface of a structured fluid film: late-stage coarsening. *Langmuir* **19**, 2419–2424.

Limat, L., Jenffer, P., Dagens, B., Touron E., Fermigier, M. & Wesfreid, J. E. 1992 Gravitational instabilities of thin liquid layers — dynamics of pattern selection. *Physica* D **61**, 166–182.

Lister, J. R., Morrison, N. F. & Rallison, J. R. 2006 Sedimentation of a two-dimensional drop towards a rigid horizontal plane. *J. Fluid Mech.* **552**, 345–351.

Lorenceau, E. & Quéré, D. 2004 Drops on a conical wire. *J. Fluid Mech.* **510**, 29–45.

Mitlin, V. S. 1993 Dewetting of solid-surface – analogy with spinodal decomposition. *J. Colloid Interface Sci.* **156**, 491–497.

Moffatt, H. K. 1977 Behaviour of a viscous film on the outer surface of a rotating cylinder. *J. Méc.* **16**, 651–673.

Newhouse, L. A. & Pozrikidis, C. 1990 The Rayleigh-Taylor instability of a viscous-liquid layer resting on a plane wall. *J. Fluid Mech.* **217**, 615–638.

Newhouse, L. A. & Pozrikidis, C. 1992 The capillary instability of annular layers and liquid threads. *J. Fluid Mech.* **242** 193–209.

Olbricht, W. L. 1996 Pore-scale prototypes of multiphase flow in porous media. *Ann. Rev. Fluid Mech.* **28** 187–213.

Oron, A., Davis, S. H. & Bankoff, S. G. 1997 Long-scale evolution of thin liquid films. *Rev. Mod. Phys.* **69**, 931–980.

Pozrikidis, C. 1990 The deformation of a liquid-drop moving normal to a plane wall. *J. Fluid Mech.* **215**, 331–363.

Quéré, D. 1990 Thin films flowing on vertical fibers. *Europhys. Lett.* **13**, 721–726.

Quéré, D. 1999 Fluid coating on a fiber. *Annu. Rev. Fluid Mech.* **31**, 347–384.

Sharma, A. & Khanna, R. 1998 Pattern formation in unstable thin liquid films. *Phys. Rev. Lett.* **81**, 3463–3466.

Tanner, L. H. 1979 The spreading of silicone drops on horizontal surfaces. *J. Physica* D **12**, 1473–1484.

Thoroddsen, S. T. & Mahadevan, L. 1997 Experimental study of coating flows in a partially-filled horizontally rotating cylinder. *Exps. Fluids* **23**, 1–13.

Trifonov, Yu. Ya. 1992 Steady-state traveling waves on the surface of a viscous liquid film falling down on vertical wires and tubes. *AIChE J.* **38**, 821–834.

Tuck, E. O. & Schwartz, L. W. 1990 A numerical and asymptotic study of some third-order ordinary differential equations relevant to coating and draining flows. *SIAM Rev.* **32**, 453–469.

Weidner, D. E., Schwartz, L. W. & Eres, M. H. 1997 Simulation of coating layer evolution and drop formation on horizontal cylinders. *J. Colloid Interface Sci.* **187**, 243–258.

Wilson, S. K. 1995 The steady thermo-capillary driven motion of a lrage droplet in a closed tube. *J. Engng Maths* **29**, 205–217.

Wu, R. & Weinbaum, S. 1982 On the development of fluid trapping beneath deformable fluid-cell membranes. *J. Fluid Mech.* **121**, 315–343.

Yiantsios, S. G. & Davis, R. H. 1990 On the buoyancy-driven motion of a drop towards a rigid surface or a deformable interface. *J. Fluid Mech.* **217**, 547–573.

Yiantsios, S. G. & Higgins, B. G. 1989 Rayleigh-Taylor instability in thin viscous films. *Phys. Fluids* A **1**, 1484–1501.